

AD-A084 129

DAVID W TAYLOR NAVAL SHIP RESEARCH AND DEVELOPMENT CE--ETC F/G 20/4
NUMERICAL OPTIMIZATION OF CIRCULATION CONTROL AIRFOILS.(U)

APR 80 T C TAI, G H KIDWELL, G N VANDERPLAATS
DTNSRDC/AERO-1265 DTNSRDC-80/060

NL

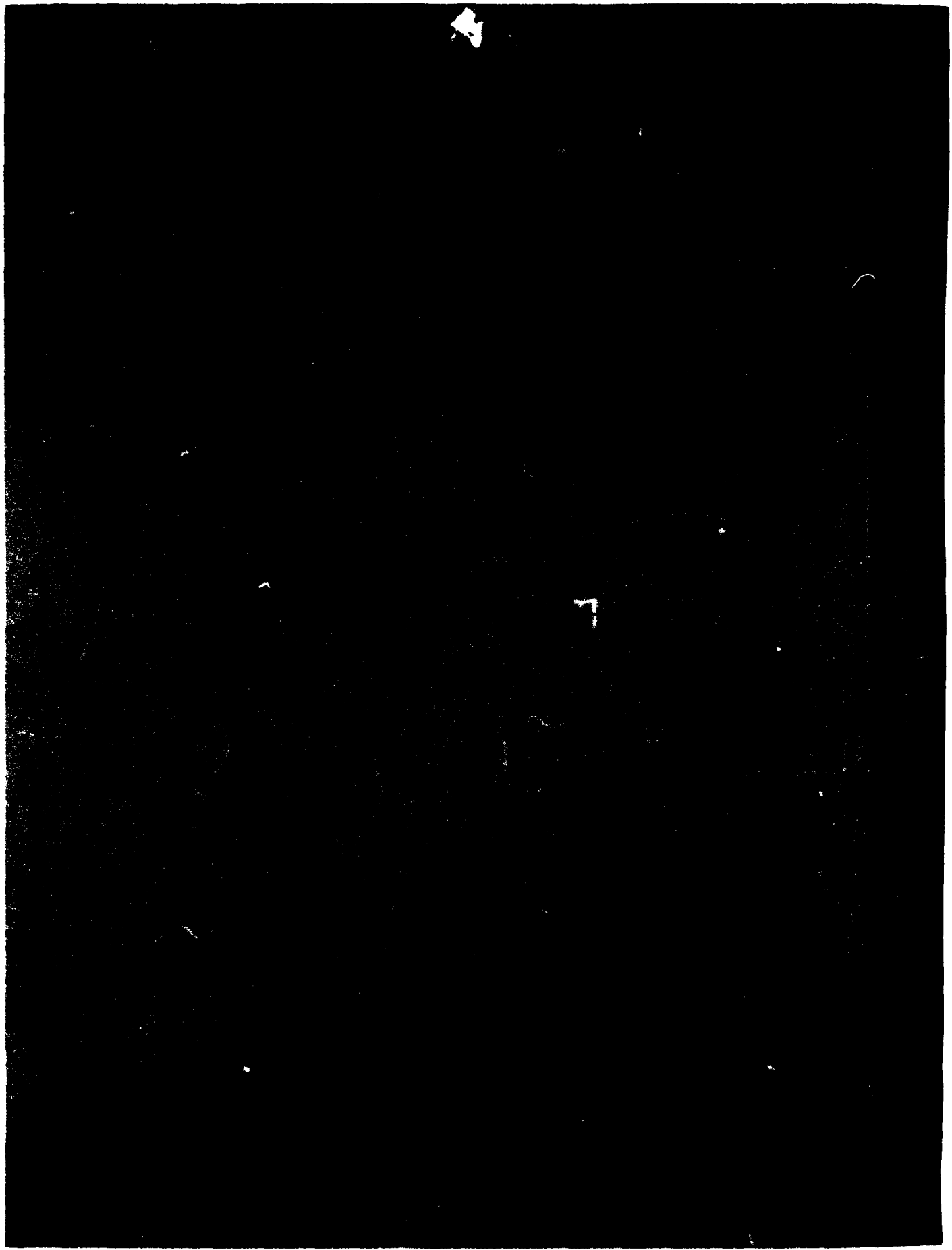
UNCLASSIFIED

1 of 1
AD
A084 129



END
DATE
FILMED
6-80
DTIC

ADA084129



UNCLASSIFIED

SECURITY CLASSIFICATION OF THIS PAGE (When Data Entered)

REPORT DOCUMENTATION PAGE		READ INSTRUCTIONS BEFORE COMPLETING FORM	
1. REPORT NUMBER DTNSRDC 801960	2. GOVT ACCESSION NO. AD-A084229	3. RECIPIENT'S CATALOG NUMBER	
4. TITLE (and Subtitle) NUMERICAL OPTIMIZATION OF CIRCULATION CONTROL AIRFOILS		5. TYPE OF REPORT & PERIOD COVERED Interim Report Sep 78-Dec 79	
7. AUTHOR(s) Tsze C./Tai, George H./Kidwell, Jr. Garret N./Vanderplaats		6. PERFORMING ORG. REPORT NUMBER Aero Report 1265	
9. PERFORMING ORGANIZATION NAME AND ADDRESS David W. Taylor Naval Ship Research and Development Center Bethesda, Maryland 20084		8. CONTRACT OR GRANT NUMBER(s) 12) 531	
11. CONTROLLING OFFICE NAME AND ADDRESS 16) ZR 02302		10. PROGRAM ELEMENT, PROJECT, TASK AREA & WORK UNIT NUMBERS (See reverse side)	
14. MONITORING AGENCY NAME & ADDRESS (if different from Controlling Office) 17) ZR 02302.01		12. REPORT DATE 11) Apr 11 1980	
16. DISTRIBUTION STATEMENT (of this Report) 14) DTNSRDC/AERO-1265 APPROVED FOR PUBLIC RELEASE. DISTRIBUTION UNLIMITED		13. NUMBER OF PAGES 50	
17. DISTRIBUTION STATEMENT (of the abstract entered in Block 20, if different from Report)		15. SECURITY CLASS. (of this report) UNCLASSIFIED	
18. SUPPLEMENTARY NOTES		15a. DECLASSIFICATION/DOWNGRADING SCHEDULE	
19. KEY WORDS (Continue on reverse side if necessary and identify by block number) Circulation Control Airfoil Numerical Optimization Incompressible Flow		Accession For NTIS GRA&I DDC TAB Unannounced Justification By Distribution/ Availability Codes Dist Avail and/or special A	
20. ABSTRACT (Continue on reverse side if necessary and identify by block number) A numerical procedure developed for optimizing the circulation control airfoils is presented. The procedure finds the optimum basic airfoil shapes subjected to specified flow conditions and geometric constraints. It consists of a numerical optimization code for linear constrained problems coupled with a viscous-potential flow interaction analysis for necessary (Continued on reverse side)			

DD FORM 1 JAN 73 1473

EDITION OF 1 NOV 65 IS OBSOLETE
S/N 0102-LF-014-6601

UNCLASSIFIED 387695

SECURITY CLASSIFICATION OF THIS PAGE (When Data Entered)

UNCLASSIFIED

SECURITY CLASSIFICATION OF THIS PAGE (When Data Entered)

(Block 10)

Task Area ZR0230201
Program Element 61152N
Work Units 1606-100 and
1606-105

(Block 20 continued)

→ viscous-inviscid flow field calculations. The desired airfoil shape is defined by a combination of baseline shapes representative of airfoils suitable for circulation control purposes. The coefficients of these basis vectors are then used as the design variables in the optimization process. Three baseline shapes (a cambered ellipse, a cambered ellipse with a drooped trailing edge, and a cambered ellipse with a logarithmically spiralled trailing edge) are employed for special contouring of the trailing edge geometry. With some minor modification of the analysis method, the combined program allows optimization for maximum lift without substantial difficulty; but for minimizing the drag, further improvement of the analysis method is required. ←

Numerical results were obtained for maximizing C_L with a blowing coefficient C_{μ} of 0.04, a Mach number of 0.3, and at angles of attack of -5 deg and -2 deg. Constraints on the lift augmentation ratio and the lift-to-drag ratio were imposed. The lift coefficient increased from an initial value of 2.05 to a final value of 2.34 for the case of $\alpha = -5$ deg. A similar result was obtained for the case of $\alpha = -2$ deg with the same flow condition. The resulting airfoil profile is somewhat between the baseline shapes of cambered ellipse and the drooped trailing edge. The result agrees qualitatively with the available experimental data for which the airfoils having cambered elliptic and drooped trailing edge contours exhibit better performance than the one with spiralled trailing edge geometry. Efforts for improving the drag prediction capability of the analysis method are in progress.

UNCLASSIFIED

SECURITY CLASSIFICATION OF THIS PAGE(When Data Entered)

TABLE OF CONTENTS

	Page
LIST OF FIGURES	iv
LIST OF TABLES	v
NOTATION	vi
ABSTRACT	1
ADMINISTRATIVE INFORMATION	1
INTRODUCTION	2
ANALYSIS METHOD	3
DVORAK-KIND METHOD	3
Potential Flow Solution	3
Laminar and Turbulent Boundary Layers	4
Viscous-Potential Flow Interaction	5
COMPUTER PROGRAM	7
COMPARISON BETWEEN THEORY AND EXPERIMENT	7
OPTIMIZATION PROGRAM	8
VANDERPLAATS METHOD	8
COMPUTER PROGRAM	9
OPTIMIZATION OF CIRCULATION CONTROL AIRFOIL	10
AIRFOIL REPRESENTATION	11
Trailing Edge Contouring	11
Overall Airfoil Shaping	12
MODIFICATION OF ANALYSIS PROGRAM	12
RESULTS AND DISCUSSION	14
CONCLUSIONS	17
ACKNOWLEDGMENT	17
REFERENCES	39

LIST OF FIGURES

	Page
1 - Flow Around a Circulation Control Airfoil	18
2 - Comparison of Calculated and Measured Lift Coefficients for a Range of Momentum Co- efficients of Model 103 Circulation Control Airfoil at $M_\infty = 0.3$ and $\alpha = -0.01$ Degree	19
3 - Comparison of Calculated and Measured Pressure Drag Coefficients for a Range of Momentum Co- efficients of Model 103 Circulation Control Airfoil at $M_\infty = 0.3$ and $\alpha = 0.01$ Degree	20
4 - Theoretical and Experimental Pressure Distributions Over Model 103 Circulation Control Airfoil at $M_\infty = 0.3$ and $\alpha = -0.01$ Degree	21
5 - Program Flow Chart	22
6 - Overlays of the Combined Program	23
7 - Three Baseline Shapes for Airfoil Representation	24
8 - Integration of Pressure Drag	25
9 - Variation of Lift and Pressure Drag Coefficients During Iteration Process for Each Analysis	26
10 - Pressure Drag Coefficients During the Course of Optimization at $M_\infty = 0.3$, $C_\mu = 0.04$, and $\alpha = -5$ Degrees	27
11 - Pressure Drag Coefficients in Two-Variable Space at $M_\infty = 0.3$, $C_\mu = 0.04$, and $\alpha = -5$ Degrees	28
12 - Lift Coefficients During the Course of Optimization at $M_\infty = 0.3$, $C_\mu = 0.04$, and $\alpha = -5$ Degrees	29
13 - Lift Coefficients in Two-Variable Space at $M_\infty = 0.3$, $C_\mu = 0.04$, and $\alpha = -5$ Degrees	30

	Page
14 - "Optimal" Airfoil Shape Resulting from Maximizing C_L at $M_\infty = 0.3$, $C_\mu = 0.04$, and $\alpha = -5$ Degrees	31
15 - Effect of Constraint in Optimization	32
16 - "Optimal" Airfoil Shape Resulting from Maximizing C_L at $M_\infty = 0.3$, $C_\mu = 0.04$, and $\alpha = -2$ Degrees	33

LIST OF TABLES

1 - Lift and Drag Coefficients of Model 103 Circulation Control Airfoil at $M_\infty = 0.3$ and $\alpha = -0.01$ Degree	34
2 - Coordinates of Baseline Airfoils	35
3 - Run Matrix for Circulation Control Airfoil Optimization Based on Baseline Shapes Y_1 , Y_2 , and Y_3	36

NOTATION

a_j	Airfoil coefficients (used as design variables)
C_c	Chordwise force coefficient
C_D	Drag coefficient (total)
C_L	Lift coefficient
C_M	Moment coefficient
C_n	Normal force coefficient
C_p	Pressure coefficient
C_μ	Momentum coefficient
c	Chord length
F	Objective function
G_j	Constraint function
h	Slot height
l	Length of a panel
M	Mach number
n	Number of panels
q	Source strength
\bar{S}	Direction of search
s	Arc length along airfoil surface
t	Thickness
V	Velocity
\bar{X}	Vector consists of design variables x_j
x, z	Airfoil coordinates

α	Angle of attack
α^*	Scalar defining distance of travel
Γ	Total circulation
γ	Vortex strength
δ^*	Boundary layer displacement thickness
ρ	Density
χ_j	Design variables

Superscripts

l	Lower
m	Iteration number during optimization
u	Upper

Subscripts

e	Edge of boundary layer
f	Frictional
i	i th panel
j	j th design variable; also jet
m	Iteration number during analysis
max	Maximum
min	Minimum
p	Pressure
$sepl$	Separation point, lower surface
$sepu$	Separation point, upper surface
∞	Freestream

ABSTRACT

A numerical procedure developed for optimizing the circulation control airfoils is presented. The procedure finds the optimum basic airfoil shapes subjected to specified flow conditions and geometric constraints. It consists of a numerical optimization code for linear or nonlinear constrained problems coupled with a viscous-potential flow interaction analysis for necessary viscous-inviscid flow field calculations. The desired airfoil shape is defined by a combination of baseline shapes representative of airfoils suitable for circulation control purposes. The coefficients of these basis vectors are then used as the design variables in the optimization process. Three baseline shapes (a cambered ellipse, a cambered ellipse with a drooped trailing edge, and a cambered ellipse with a logarithmically spiralled trailing edge) are employed for special contouring of the trailing edge geometry. With some minor modification of the analysis method, the combined program allows optimization for maximum lift without substantial difficulty; but for minimizing the drag, further improvement of the analysis method is required.

Numerical results were obtained for maximizing C_L with a blowing coefficient C_μ of 0.04, a Mach number of 0.3, and at angles of attack of -5 deg and -2 deg. Constraints on the lift augmentation ratio and the lift-to-drag ratio were imposed. The lift coefficient increased from an initial value of 2.05 to a final value of 2.34 for the case of $\alpha = -5$ deg. A similar result was obtained for the case of $\alpha = -2$ deg with the same flow condition. The resulting airfoil profile is somewhat between the baseline shapes of cambered ellipse and the drooped trailing edge. The result agrees qualitatively with the available experimental data for which the airfoils having cambered elliptic and drooped trailing edge contours exhibit better performance than the one with spiralled trailing edge geometry. Efforts for improving the drag prediction capability of the analysis method are in progress.

ADMINISTRATIVE INFORMATION

The work presented in this report was supported by the Independent Research Program at the David W. Taylor Naval Ship Research and Development Center (DTNSRDC) under Work Units 1606-100 and 1606-105. NASA Ames Research Center has provided computer support in cooperation with its V/STOL Systems Office under the direction of Mr. A. Faye.

INTRODUCTION

In the development of technology for V/STOL aircraft, efforts have been made to increase the lift coefficient through blowing. Systems which use blowing may be classified into three major categories: (1) the blowing flap, (2) the jet flap, and (3) the circulation control airfoils. In the application of blowing to helicopter rotors, the circulation control (CC) system offers two basic advantages, namely, the much higher lift-to-thrust augmentation for a given slot momentum and the mechanical simplifications in lift control.

Experimental data are available for circulation control airfoils.^{1*,2-4**} Analytical methods developed earlier used an integral approach to model the flow as an incompressible turbulent boundary layer flow mixed with a wall jet.^{5,6} Later, Dvorak and Kind solved the wall jet flow region problem by the finite difference scheme but retained the integral approach for flow regions where ordinary boundary layers prevail.⁷ Reasonably good lift-momentum results have been reported in using these methods, although a major deficiency in drag prediction still exists. Attempts to incorporate a more realistic eddy viscosity model are found elsewhere.⁸

To meet the performance requirement for several naval applications,^{***} an optimization procedure is highly desirable to provide an advanced design capability. In the present work, a numerical approach is taken to optimize the airfoil for maximum lift or for minimum drag, or for maximum lift-to-drag ratio. Various constraints including thickness, lift-to-drag ratio, and lift-momentum flux relations are imposed to generate optimal airfoil shapes. In so doing, a numerical optimization scheme of Vanderplaats⁹ for linear or nonlinear constrained problems has been employed and coupled with a viscous-potential flow interaction analysis of Dvorak and Kind⁷ for necessary viscous-inviscid flow field calculations.

*A complete listing of references is given on page 39.

**Work performed by J.S. Abramson for two-dimensional subsonic wind tunnel tests of the circulation control airfoils documented as DTNSRDC TM-16-76-42 of December 1975.

***During 1977 to 1979, the circulation control airfoils have been applied to an A-6 testbed aircraft, an H-2 helicopter, and a stopped rotor (X-Wing) aircraft at DTNSRDC.

Reasonably good agreement between theoretical and experimental results for certain cases has been reported to warrant some confidence in the method.

ANALYSIS METHOD

A schematic of the flow about a CC airfoil is shown in Figure 1. As opposed to the conventional airfoil, a typical CC airfoil is equipped with a blowing slot on the upper surface for energizing the flow in the viscous layer and a rounded trailing edge for deflecting the jet. High lift can be generated because of increased circulation created by the blowing jet. The flow is characterized by outer inviscid flow and inner viscous flow consisting of boundary layers, wall jet, and separation bubble.

Rather than starting from scratch, the analysis method developed by Dvorak and Kind⁷ with some minor modifications was adopted. The method is found to be the most comprehensive one available. A brief description of the theory is given below.

DVORAK-KIND METHOD

Dvorak and Kind⁷ considered the subject problem as a viscous-inviscid interaction flow over a two-dimensional airfoil section with or without slot blowing on the upper surface. The inviscid potential flow is calculated first and then followed by boundary layer and wall jet developments which are computed using pressure distributions obtained from the potential flow analysis. The viscous effects are modeled and the procedure is repeated until a converged solution is achieved.

Potential Flow Solution

The potential flow is represented by vorticity distribution along the panels. The vortex strength is assumed to vary linearly along each panel and is continuous at all junction points. The horizontal and vertical component of the velocity induced by the vorticity according to the potential flow theory is

$$u = \frac{\gamma}{2\pi} \left\{ \frac{z}{c} \log \frac{\sqrt{(x-c)^2 + z^2}}{\sqrt{x^2 + z^2}} - \frac{x}{c} \left[\tan^{-1} \frac{z}{x} - \tan^{-1} \frac{z}{x-c} \right] \right\} \quad (1)$$

$$w = \frac{\gamma}{2\pi} \left\{ 1 + \frac{z}{c} \left[\tan^{-1} \frac{z}{x} - \tan^{-1} \frac{z}{x-c} \right] + \frac{x}{c} \log \frac{\sqrt{(x-c)^2 + z^2}}{\sqrt{x^2 + z^2}} \right\} \quad (2)$$

where γ is the vortex strength along the panel. The solution procedure is similar to those for conventional airfoils except that the Kutta condition is applied differently. For a rounded trailing edge, which is typical in a CC airfoil, the Kutta condition is replaced by an equation which specifies the value of the total circulation Γ around the airfoil

$$\Gamma = \sum_{i=1}^N \left[\ell_i \frac{(\gamma_i + \gamma_{i+1})}{2} \right] \quad (3)$$

where ℓ_i is the length of the i th panel. The value of Γ , together with the blowing coefficient C_{μ} , has direct bearing on the lift coefficient. A detailed description of the potential flow solution can be found in Reference 10.

Laminar and Turbulent Boundary Layers

The forward and aft stagnation points obtained by the potential flow solution divide the flows between the upper and lower surfaces of the airfoil. Based on pressures obtained from the potential flow solution, calculation of boundary layers starts with the Hiemenz stagnation flow solution.¹¹ Curle's¹² integral method is employed for calculating the laminar boundary layers downstream of the stagnation point for both upper and lower surfaces. After the transition predicted by Granville's empirical formula,¹³ the turbulent boundary layers for the remaining lower surface to the separation point, and the upper surface to the blowing slot

are calculated using the Nash-Hicks integral method.¹⁴ At the slot, the turbulent boundary layer mixes with a wall jet of a uniform velocity distribution. A finite difference scheme is used in solving the mixed flow. The flow proceeds around a highly curved surface with very strong adverse pressure gradients. The effect of surface curvature downstream of the blowing slot is accounted for by including the normal momentum equation for radial variation of static pressure in the finite difference procedure. The flow eventually separates after passing the blunted trailing edge and a separation pressure is noted.

Viscous-Potential Flow Interaction

The viscous effects produced by the boundary layer development are modeled by a source distribution along the airfoil surface. The source strength q_i at any junction point of a surface panel is obtained by

$$q_i = \frac{d}{ds} (V_e \delta^*) \quad (4)$$

where s = arc length

V_e = local external velocity

δ^* = boundary-layer displacement thickness

Equation (4) applies to the conventional boundary layers as well as to the wall jet. In the latter case, the product $V_e \delta^*$ tends to decrease, yielding a negative source strength (i.e., sink).

The contribution of q_i is then implemented in the potential flow solution which alters the results of the pressure distribution. The entire procedure is then repeated with subsequent values of the total circulation estimated by

$$\Gamma_{m+1} = \Gamma_m + k \left(C_{P_{sepu}} - C_{P_{sepl}} \right) \quad (5)$$

where the numerical constant k has a value from 0.1 to 0.3. The calculations are terminated when the lift coefficient, which is directly related to the Γ_{m+1} value, remains within a specified tolerance and, at the same time, the differences in pressure coefficients at the upper and lower ends of the separation bubble, $(C_{p_{sepu}} - C_{p_{sepl}})$ diminish.

The lift and pressure drag coefficients are then evaluated by integrating the surface pressure distribution using the trapezoidal rule

$$C_n = \sum_{i=1}^{N+1} \frac{(C_{p_{i+1}} + C_{p_i})(x_{i+1} - x_i)}{2}$$

$$C_c = \sum_{i=1}^{N+1} \frac{(C_{p_{i+1}} + C_{p_i})(z_{i+1} - z_i)}{2} \quad (6)$$

$$C_L = C_n \cos \alpha - C_c \sin \alpha; \quad C_{D_p} = C_n \sin \alpha + C_c \cos \alpha$$

where x and z are airfoil coordinates normalized by the chord length, and N is the number of panels. The total drag is the sum of the pressure drag and skin friction, less the blowing momentum coefficient

$$C_D = C_{D_p} + C_{D_f} - C_\mu \quad (7)$$

The momentum coefficient is defined by

$$C_\mu \equiv \frac{\rho_j v_j^2 h}{\frac{1}{2} \rho_\infty v_\infty^2 c} \quad (8)$$

where $\rho_j v_j^2$ is the momentum flux of the blowing jet and h is the jet height at the slot.

COMPUTER PROGRAM

The method has been coded in FORTRAN and is known as the CIRCON program. It has been written in an overlay form to reduce core requirements. A detailed description of the code can be found in Reference 15.

COMPARISON BETWEEN THEORY AND EXPERIMENT

Previous results of the Dvorak-Kind method, reported in Reference 7 show good agreement between the theory and the experiment. Cases considered in Reference 7 include comparison of the computed results with experimental data of a cambered 20-percent ellipse.

The method has been applied to other cases at DTNSRDC on different airfoils with various flow conditions, among which is discussed the case of a 15-percent cambered ellipse at $M_\infty = 0.3$ and $\alpha = -0.01$ deg. The computed results are compared with experimental data* obtained at the DTNSRDC 7 ft \times 10 ft transonic wind tunnel where the blockage effects can be considered insignificant at moderate blowing conditions. The results are given in Table 1. Figures 2 and 3 show the calculated lift and drag coefficients at various blowing conditions between $C_\mu = 0.0073$ and 0.0384, along with experimental data. Qualitative agreement between the theoretical and experimental lift coefficients is obtained. However, serious discrepancies in drag coefficients are observed. In particular, the dip in the theoretical drag curve is not detected in the experiment. Some representative pressure distributions (for $C_\mu = 0.0111, 0.0160,$ and 0.0220) are given in Figure 4, which may reveal the disagreement.

The results indicate that although the Dvorak-Kind method is the most sophisticated approach available for analyzing the flow over a CC airfoil, it is still inadequate. Efforts in numerical optimization here, discussed later, will be restricted to the cases using the lift coefficient as the objective function to obtain optimal shapes. Nonetheless, the approach is capable of achieving qualitative results which may be used to guide the design engineers.

*Experimental data were provided by J.B. Wilkerson and J.S. Abramson of DTNSRDC.

OPTIMIZATION PROGRAM

The aforementioned analysis method has been coupled with a numerical optimization scheme developed by Vanderplaats.⁹ A brief description of the optimization technique is given here and the procedure for automating the CC airfoil design is outlined.

VANDERPLAATS METHOD

The optimization program is based on the method of feasible directions for constrained problems. The optimization problem is stated mathematically as

$$\text{Minimize OBJ} = F(\bar{X})$$

which is subject to:

$$G_j(\bar{X}) \leq 0 \quad (j=1,m) \quad (9)$$

$$X_j^l \leq X \leq X^u \quad (j=1,n) \quad (10)$$

where OBJ is the objective function. The vector \bar{X} contains n design variables. The function $G_j(\bar{X})$ defines the constraints which the designer wishes to impose on the optimization problem. Functions $F(\bar{X})$ and $G_j(\bar{X})$ may be either implicit or explicit of the design variables \bar{X} but must be continuous. Variables X_j^l and X_j^u define the lower and upper bounds, respectively, on the design variable and are the limits over which $F(\bar{X})$ and $G_j(\bar{X})$ are defined. If the inequality condition of Equation (9) is violated ($G_j(\bar{X}) > 0$) for any constraint, the constraint is said to be violated. If the equality condition is met ($G_j(\bar{X}) = 0$), the constraint is called active, and if the strict inequality is met ($G_j(\bar{X}) < 0$), the constraint is inactive. Because a precise zero is seldom meaningful in the digital computation, a constraint is called active if its value is within a specified tolerance.

The n-dimensional space spanned by the design variables \bar{X} is referred to as the design space. Any design which satisfies the inequalities of Equations (9) and (10) is referred to as a feasible design. If a design violates one or more of these inequalities, it is said to be infeasible. The minimum feasible design is said to be optimal. Note that if one wishes to maximize some function such as lift, it can be done simply by minimizing the negative of lift. Thus, any design problem can be cast in the foregoing form.

The optimization program begins with an initial \bar{X} vector which is input to the program and may or may not define a feasible design. The optimization process then proceeds iteratively by the following recursive relationship

$$\bar{X}^{m+1} = \bar{X} + \alpha^* \bar{S}^m \quad (11)$$

where m = iteration number

\bar{S} (vector) = direction of search in the n-dimensional design space

α^* = scalar which defines the distance of travel in direction \bar{S}

The \bar{S}^m is obtained by moving in the direction of the steepest descent (the negative gradient of the objective function) without violating constraints. The scalar α^* is determined by a one-variable search based on a polynomial fit of several trial values.

The procedure is repeated with the aid of a conjugate direction algorithm¹⁶ in determining the new search direction. When the constraint is encountered in the searching process, the new search direction is found using Zoutendijk's method of feasible directions.¹⁷ The optimum point is achieved where no direction can be found that will reduce the objective without violating the constraints.

COMPUTER PROGRAM

The optimization procedure is coded in FORTRAN known as CONMIN.⁹ The program has been expanded since its first appearance in 1973. A main

control program known as COPES having four modes of application, namely, ANALYSIS, SENSITIVITY STUDY, TWO-VARIABLE SPACE, and OPTIMIZATION is now available. Also an approximation optimization procedure is added using a truncated Taylor's series to reduce the number of required analyses. Both old and new versions have been widely used in various engineering disciplines.

OPTIMIZATION OF CIRCULATION CONTROL AIRFOIL

The subject problem is to optimize the airfoil for maximum lift, or for minimum drag, or for maximum lift-to-drag ratio. Various constraints including minimum lift range, maximum drag range, angle of attack, lift augmentation ratio, thickness ratio, jet detachment, and linear lift-momentum flux relations are to be imposed to generate optimal airfoil shapes.

The optimization model for the problem contains the objective, the constraints, and the design variables. For example, if we want to optimize the airfoil for maximum lift subject to thickness ratio and lift-to-drag ratio constraints, the optimization model would be

$$\text{Objective - } F(\bar{X}): \quad - C_L$$

$$\text{Constraints - } G(\bar{X}): \quad (t/c)_{\min} \leq t/c \leq (t/c)_{\max} \quad (12)$$

$$(C_L/C_D)_{\min} \leq C_L/C_D \leq (C_L/C_D)_{\max} \quad (13)$$

$$\text{Design Variables - } \bar{X}: \quad a_j, \quad j = 1, n$$

where the variables a_j are the coefficients of a linear combination of n baseline airfoils that represent the design airfoil:

$$Y = \sum_{j=1}^n a_j Y_j \quad (14)$$

The lift coefficient C_L and the drag coefficient C_D are nonlinear implicit functions of the design variables to be obtained by the analysis method and the thickness ratio is a linear function of the design variables determined directly by Equation (14).

The model is implemented numerically by interaction between the optimization and airfoil analysis programs. The program flow chart for such an operation is shown in Figure 5. In so doing, the airfoil analysis program CIRCON is merged with the optimization code CONMIN on the CDC 7600 computer at the NASA Ames Research Center to form an airfoil design capability. The overlay of the combined program is shown in Figure 6. The program can be operated either at Ames or at DTNSRDC using a remote terminal.

AIRFOIL REPRESENTATION

Trailing Edge Contouring

The trailing edge geometry has direct bearing on the jet deflection characteristics and, therefore, our first effort is to contour the blunt trailing edge of the CC airfoil. Three baseline shapes, i.e., those of a cambered ellipse, a cambered ellipse with a drooped trailing edge, and a cambered ellipse with a logarithmically spiralled trailing edge,* are employed in test cases. These shapes (shown in Figure 7), representative of airfoils suitable for circulation control purposes, allow special contouring of the trailing edge geometry which directly affects the airfoil performance. Equation (10), therefore, simplifies to

$$Y = a_1 Y_1 + a_2 Y_2 + a_3 Y_3 \quad (15)$$

The exact coordinates of these baseline airfoils are listed in Table 2.

All three shapes have identical coordinates up to $x/c = 0.95$. Variation is allowed between $0.95 \leq x/c \leq 1.00$. For this special case, since the thickness of the resulting airfoil remains constant, we have

*These baseline shapes are provided by E.O. Rogers of the Aviation and Surface Effects Department, DTNSRDC.

$$a_1 + a_2 + a_3 = 1 \quad (16)$$

Accordingly, Equation (15) can be written as

$$Y = a_1 Y_1 + a_2 Y_2 + (1-a_1-a_2) Y_3 \quad (17)$$

The new form of Equation (17) reduces the actual number of design variables from three to two (but still three baseline shapes). It, in turn, reduces the number of gradients and, thus, simplifies the search process. It also eliminates the thickness constraint, which is automatically satisfied. Note that since negative values of a_1 , a_2 , or a_3 are allowed, the resulting airfoil shape can be drastically different from these original profiles.

Overall Airfoil Shaping

The ultimate purpose of the present work is to derive a CC airfoil for optimum performance. The work involves overall airfoil shaping based on more general representation of baseline profiles. The computer program has been set up to accept as many as twenty-five (25) baseline shapes, although practically six would be sufficient to cover a broad range of interest.

MODIFICATION OF ANALYSIS PROGRAM

A major difficulty in using the viscous-inviscid interaction method together with the optimization code, however, is its inability in providing fairly smooth gradients of the objective function when the design variables are perturbed in the course of optimization. The problem is a common one in most viscous-inviscid interaction methods in which the viscous and inviscid flows are calculated separately and the final solution is reached by the iterative process. In addition, as mentioned earlier, the correlation between the analysis method and the experiment requires further improvement. The problem is, therefore, twofold, i.e., convergence and accuracy.

To circumvent the problem, some modifications to the analysis program need to be carried out. The approach is to make the program operational with the least modification required and then to refine it as necessary.

The first step is, therefore, to smooth out some irregularities in aerodynamic force coefficients, which might be partially caused by the simple trapezoidal rule used in integrating the surface pressure distribution on a limited number of panels. Equation (6) is thus replaced by a second-order Lagrangian interpolation scheme for the integrand, which results in

$$C_n = \sum_{i=1}^{N+1} \left\{ C_{P_i} \left[\frac{x_{i+1} - x_{i-1}}{x_i - x_{i-1}} + 2 \right] + C_{P_{i+1}} \left[\frac{x_i - x_{i-1}}{x_{i+1} - x_{i-1}} + 2 \right] - C_{P_{i-1}} \left[\frac{(x_{i+1} - x_i)^2}{(x_i - x_{i-1})(x_{i+1} - x_{i-1})} \right] \right\} \frac{(x_{i+1} - x_i)}{6} \quad (18)$$

For evaluating C_c , x 's are replaced by z 's.

The difference between the two schemes can be appreciable in drag values attributed to the leading and trailing edge regions where change in sign of the pressure coefficient takes place. Figures 8a and 8b indicate the C_D values (the net areas, which are the differences of the shaded regions) resulting from these two schemes. The advantage of using the Lagrangian scheme is twofold: (a) improving the convergences of C_L values and (b) improving the accuracy for both C_L and C_D . This is shown in Figure 9. The slope of the C_L variation during the iteration for the Lagrangian scheme is smaller than that for the trapezoidal rule. After eight iterations by using Equation (18), the resulting C_L (converged since $\Delta C_L / C_L \leq \epsilon$ where ϵ is a specified tolerance) is smaller, but C_D is larger, than it would be if using Equation (6). The accuracy of both C_L and C_D has been improved since the theory overpredicts the lift but underpredicts the drag (see Figures 2 and 3). It is anticipated that if a large number of panels is used, the difference between the two schemes should be minimal.

The modification (although a minor one), when coupled with the recast equation for airfoil representation (Equation (17)), allows performing optimization runs for maximizing the lift without substantial difficulty; but for minimizing the drag, further improvement of the analysis method is required. This will be discussed further in the next section.

The second phase of the effort, which is now in progress, will be concentrated on modifications of the analysis program including (a) remodeling the potential flow solution to consider the effect of the large wake associated with the blowing jet and (b) removal of the assumption of constant pressure inside the separation bubble which has caused some arbitrary variation in aerodynamic force coefficients. Although only slightly noticeable in lift coefficients, these variations produce widespread differences in drag values. Finally, (c) rearrangement of the viscous-potential flow interaction procedure to improve convergence of the overall solution.

RESULTS AND DISCUSSION

Numerical results were calculated on the NASA Ames CDC 7600 computer using a remote terminal at DTNSRDC. The merged program was first checked by the ANALYSIS, SENSITIVITY STUDY, and TWO-VARIABLE SPACE runs in accordance with the control options of the main program COPES before extensive OPTIMIZATION runs were performed. Results of the ANALYSIS runs are tabulated in Table 1, plotted in Figures 2, 3, and 4, and have been discussed previously in the Analysis Method section. Results of other typical runs are summarized in Table 3 and presented in Figures 10 through 16.

The first optimization run was a simple case for minimizing the frictional drag with the angle of attack as the design variable. The results of this run yield a slight decrease in skin friction corresponding to a change of the design variable α from -5 deg to -4.9 deg. The purpose of the run was to test the status of the program rather than actually design for minimum skin friction, which is just a small portion of the total drag and has only a small range of variation.

The next two runs were aimed at minimizing the total drag subject to constraints of C_L/C_μ , C_{D_T}/C_L , and t/c values (Runs 6 and 7 in Table 3). The angle of attack was used as the design variable for Run 6, and the coefficients a_1 , a_2 , and a_3 for Run 7. Unfortunately, there was no change in the objective function for either case.

Since the skin friction values remain fairly constant, the variation of the total drag is basically attributed to the variation of the pressure drag. From Runs 8 through 10, therefore, the pressure drag, which is more direct than the total drag, was employed as the objective function under similar constraints. With the aid of the recasted airfoil equation and the modifications in the integration scheme of the analysis method, a moderate change in the pressure drag is obtained in Run 10b, as shown in Figure 10. The advantage of using the Lagrangian scheme is clearly demonstrated in Figure 10 although the general outcome in these cases appears not as good as anticipated.

The problem in minimizing the drag can best be understood by the plot of the C_{D_p} value in two-variable space given in Figure 11. The zigzag C_{D_p} distribution throughout the $a_1 - a_2$ space cannot provide smooth values of gradients $\partial C_{D_p} / \partial a_1$, and $\partial C_{D_p} / \partial a_2$ and, therefore, the optimization technique fails to respond properly when a_1 and a_2 are perturbed. There are, however, still some regions where local continuity of the gradients exists. These permit changes in the objective function during the course of optimization, such as those shown in Figure 10. Nevertheless, the result of Figure 10 can only be regarded at best, as locally optimal; its usefulness is very limited.

Subsequent efforts were concentrated on cases using the lift coefficient as the objective. Numerical results were obtained for maximizing C_L with a blowing coefficient C_μ of 0.04, at a Mach number of 0.3, and at angles of attack of -5 deg and -2 deg. Constraints of the lift augmentation ratio, $50 \leq C_L/C_\mu \leq 60$, and the lift-to-drag ratio, $-0.014 \leq C_D/C_L \leq -0.006$, were imposed. Figure 12 shows the values of C_L versus the search position during the course of optimization for the case of

$\alpha = -5$ deg. The search starts with $a_1 = 0.3333$ and $a_2 = 0.3334$, which yields $C_L = 2.054$. The search stops after the change of the objective function within a specified tolerance, consecutively for three times. A final lift coefficient of 2.34, is achieved (Run 12 in Table 3) with design variables $a_1 = 0.4084$, $a_2 = 0.4798$, and $a_3 = 0.1180$. A similar run with less restrictive constraints, but using three design variables along with the original trapezoidal rule integration (Run 11a in Table 3), is also plotted in Figure 12. Again, it indicates that the advantage of using the recast airfoil equations along with the Lagrangian scheme is distinctive.

Figure 13 shows the C_L values in the two-variable design space. Continuity of C_L values in most regions is maintained, as marked by solid lines. Some uncertainty is involved in the region with broken lines. As a double check, the intermediate C_L values of Run 12 are superimposed in Figure 13. Figure 13 indicates that the optimal value approaches the true maximum fairly closely. The C_L value tends toward but terminates before the maximum because the termination criterion has been met. The test warrants further extension to more baseline shapes in representing the airfoil so that greater versatility may be achieved.

The resulting airfoil profile, which is shown in Figure 14, is somewhat between baseline shapes Y_1 and Y_2 . The result agrees qualitatively with the available experimental data for which the airfoils having cambered elliptic and drooped trailing edge contours exhibit better performance than the spiralled one. It is of interest to note that at negative angles of attack, where the CC airfoils normally operate, high C_L values are usually accompanied by low drag coefficients.

Figure 15 shows C_L values during the optimization process for the case of $M_\infty = 0.3$, $C_\mu = 0.04$, and $\alpha = -2$ deg. The calculation was terminated after five searches: the C_L values gained from 2.255 to 2.740 (Run 13 in Table 3). The final design ended up with $a_1 = 0.499$, $a_2 = 0.624$, and $a_3 = -0.123$. The resulting airfoil is depicted in Figure 16. Note that a_3 has a negative value, which yields a more drooped trailing edge than the previous case of $\alpha = -5$ deg.

Finally, the effect of the constraint on the resulting C_L values is examined. This is shown in Figure 15, where the results of Run 14 (with constraints encountered during the course of optimization) are compared with those of Run 13 (without constraints encountered). Considerable penalty due to the active constraints are realized.

CONCLUSIONS

A numerical procedure for optimizing circulation control airfoils is developed. Based on the first phase of work in the continuing effort of improving aerodynamic performance of the circulation control airfoil--the following conclusions may be drawn:

1. A significant gain (about 12 to 15 percent) in lift coefficients of CC airfoils may be achieved by optimizing the trailing edge contour. It was found that, in the range of small negative angles of attack, the drooped trailing edge yields better aerodynamic performance than the spiralled one.

2. A major difficulty in using the viscous-inviscid interaction method along with the optimization code is its inability to provide fairly smooth gradients of the objective function. It is possible, however, to make optimum calculations for maximum lift by reducing the number of design variables to the minimum and removing some irregularities in the integration of aerodynamic force coefficients from the surface pressure distribution. For minimizing the drag, further improvement of the analysis method is required.

3. Based on a limited comparison of the theoretical results with experimental data obtained with negligible wall blockage effect, it was found that the Dvorak-Kind method overpredicts the lift but underpredicts the drag.

ACKNOWLEDGMENT

The authors would like to acknowledge the assistance provided by E.O. Rogers, J.S. Abramson, and J.B. Wilkerson (Code 1603) during the course of the present work and some enlightening discussions with R.M. Williams, S. de los Santos (Code 1606), and D.A. Jewell (Code 012.3), all of DTNSRDC.

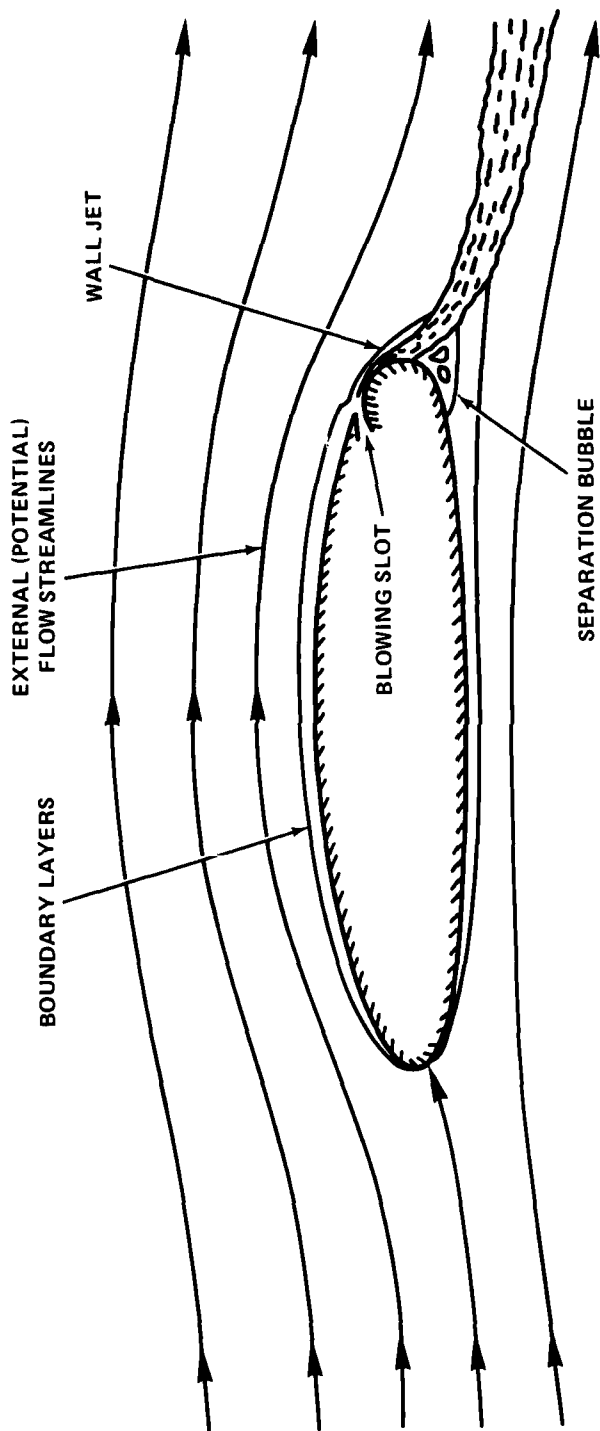


Figure 1 - Flow Around a Circulation Control Airfoil

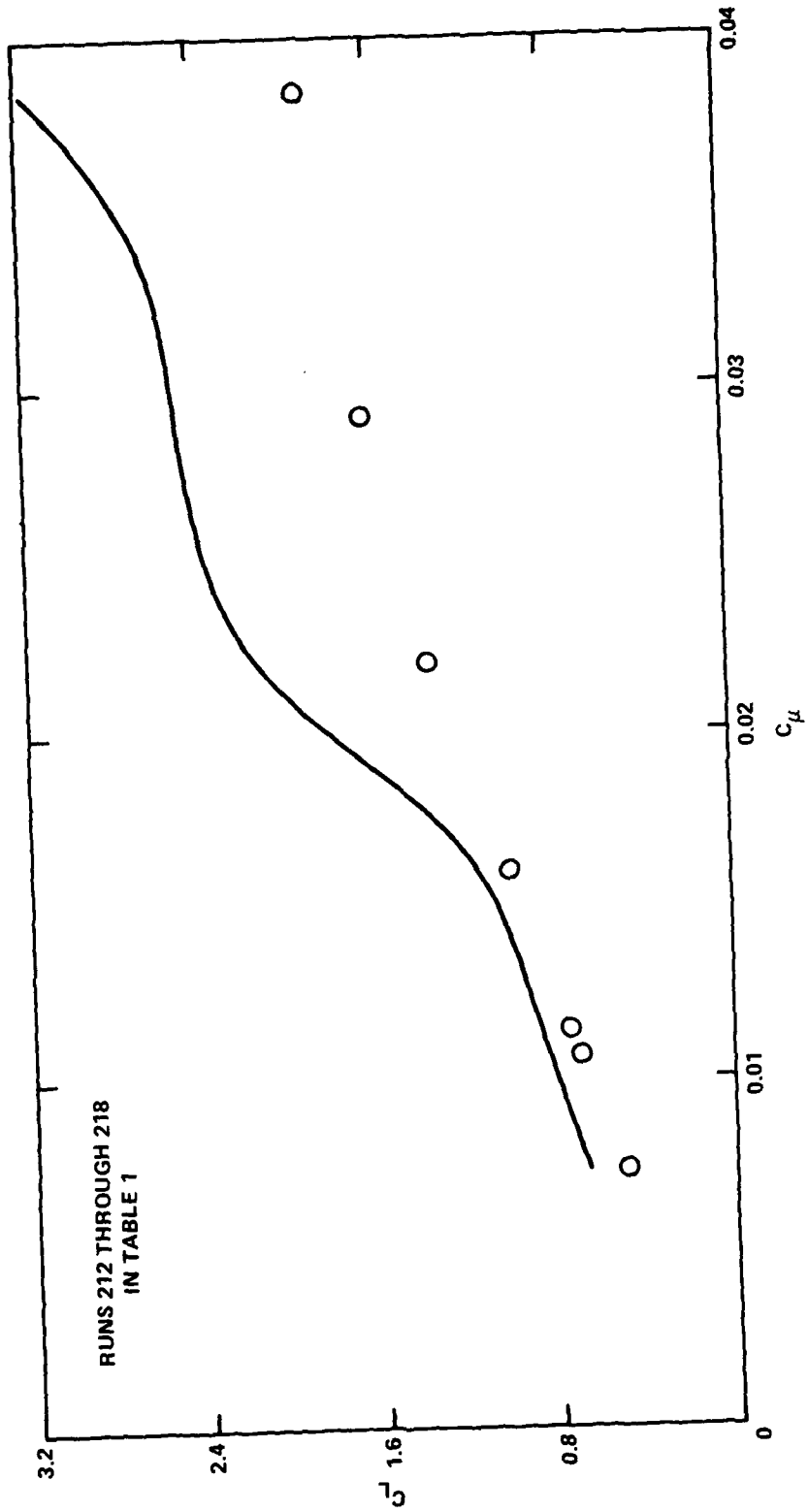


Figure 2 - Comparison of Calculated and Measured Lift Coefficients for a Range of Momentum Coefficients of Model 103 Circulation Control Airfoil at $M_{\infty} = 0.3$ and $\alpha = -0.01$ Degree

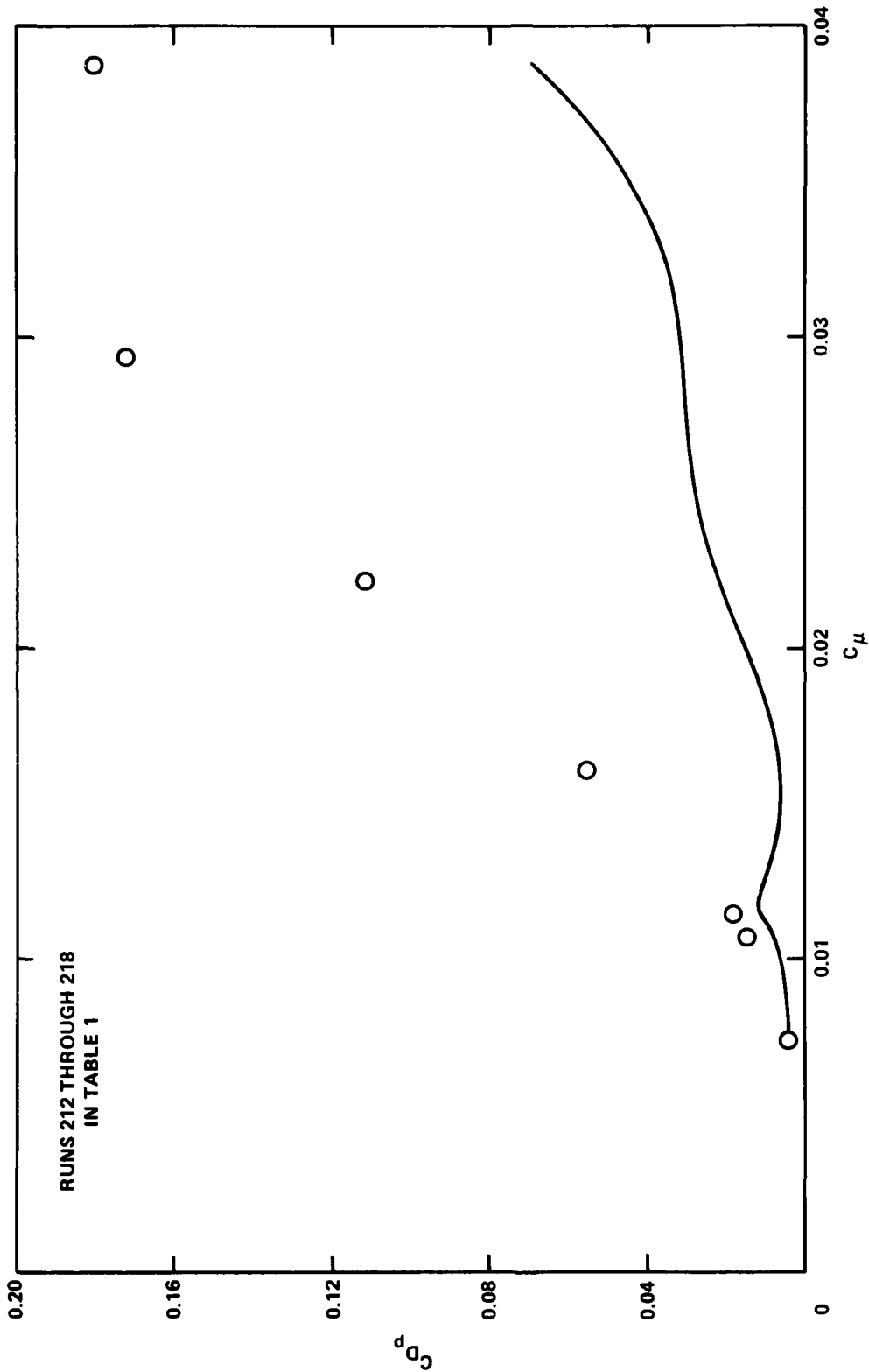


Figure 3 - Comparison of Calculated and Measured Pressure Drag Coefficients for a Range of Momentum Coefficients of Model 103 Circulation Control Airfoil at $M_\infty = 0.3$ and $\alpha = 0.01$ Degree

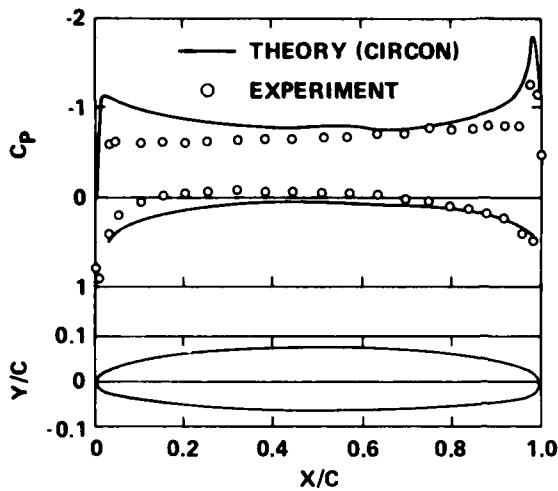


Figure 4a - $C_{\mu} = 0.0111$

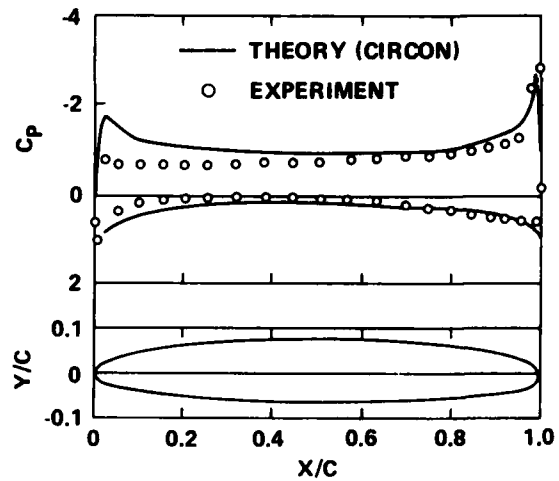


Figure 4b - $C_{\mu} = 0.0160$

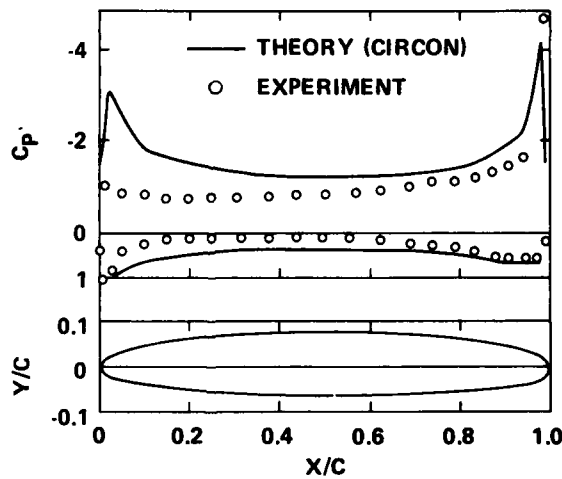


Figure 4c - $C_{\mu} = 0.0220$

Figure 4 - Theoretical and Experimental Pressure Distributions Over Model 103 Circulation Control Airfoil at $M_{\infty} = 0.3$ and $\alpha = -0.01$ Degree

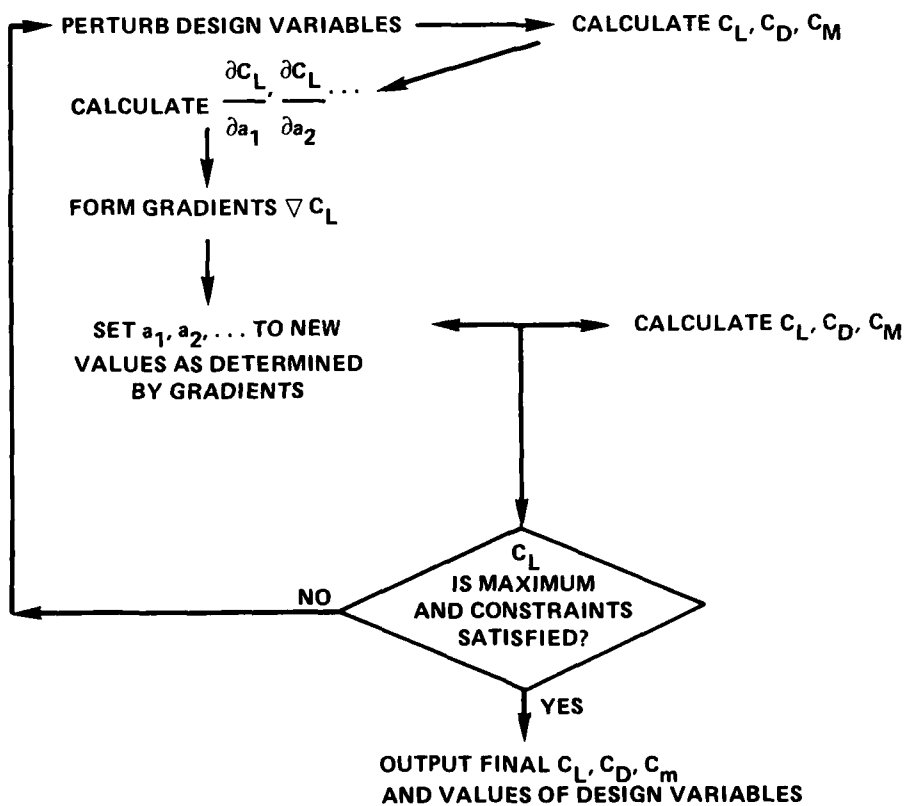
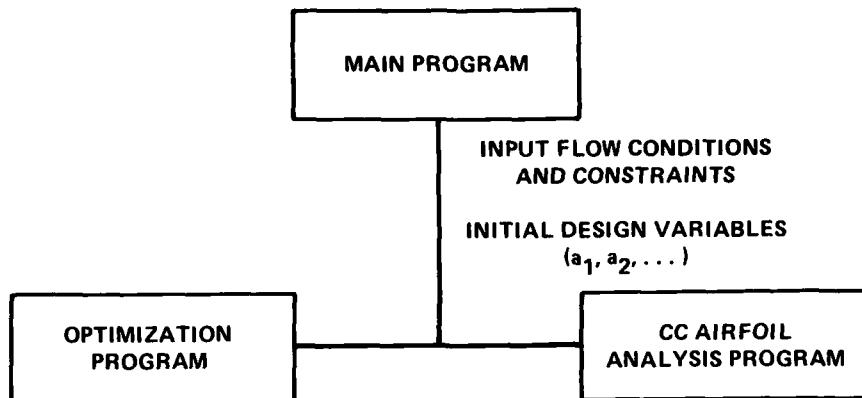


Figure 5 - Program Flow Chart

NUMERICAL OPTIMIZATION PROGRAM
FOR
CIRCULATION CONTROL AIRFOIL SHAPES

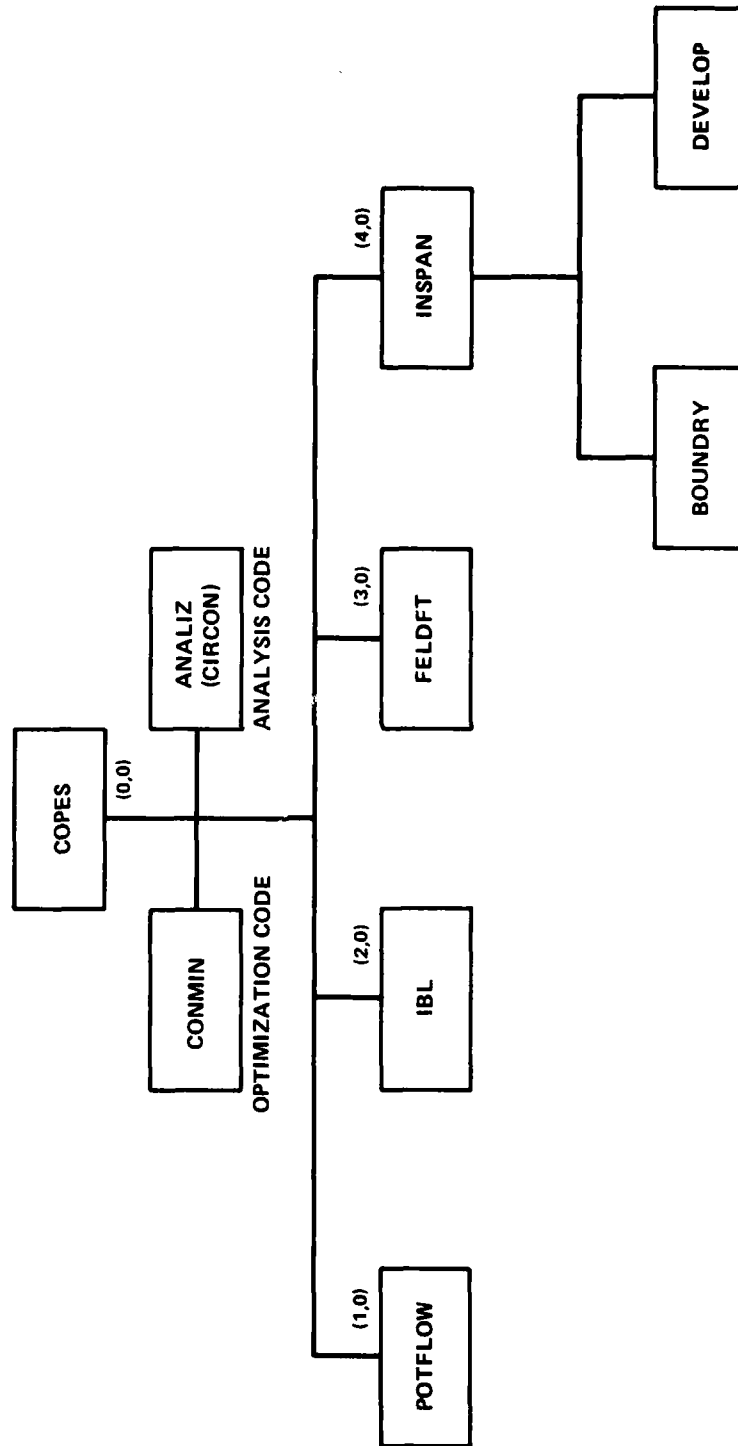
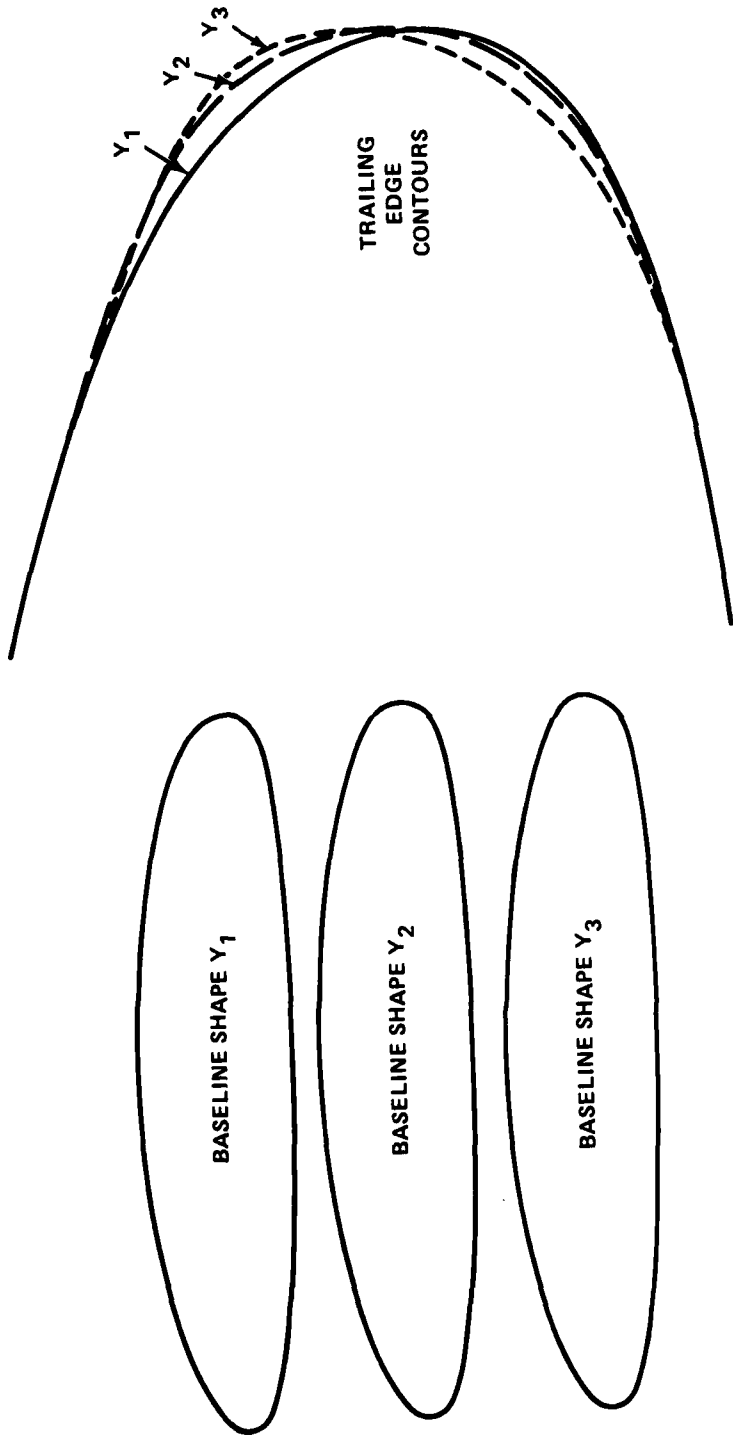


Figure 6 - Overlays of the Combined Program



AIRFOIL REPRESENTATION: $y = a_1 Y_1 + a_2 Y_2 + a_3 Y_3$

Figure 7 - Three Baseline Shapes for Airfoil Representation

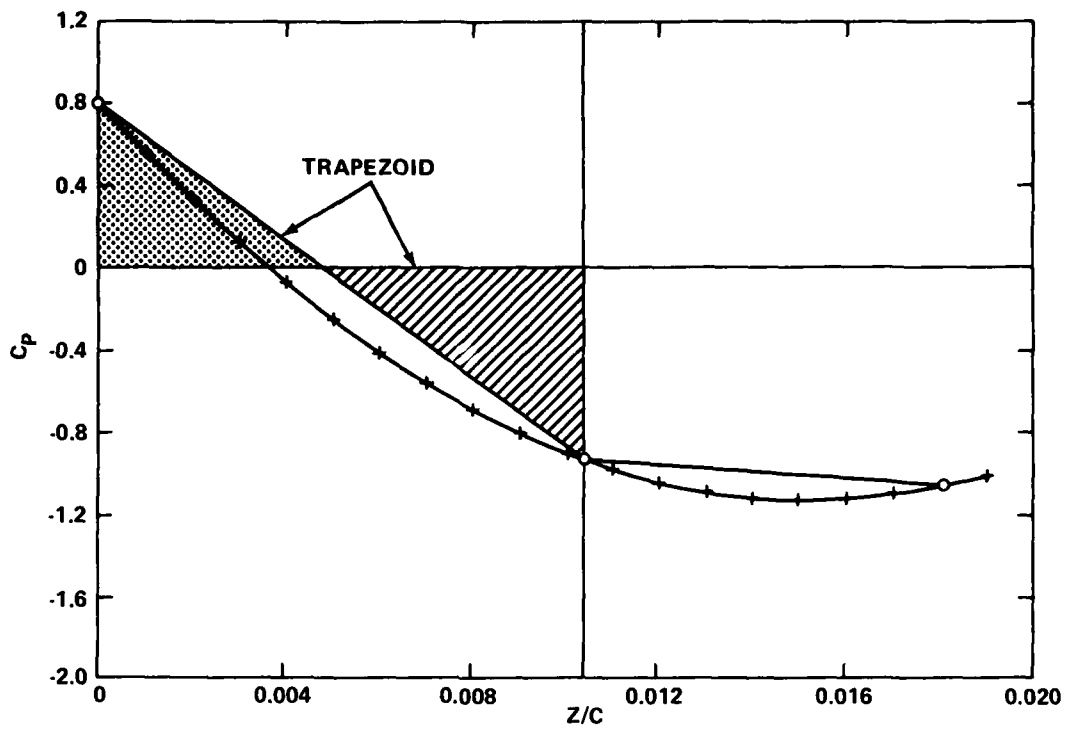


Figure 8a - Trapezoidal Rule

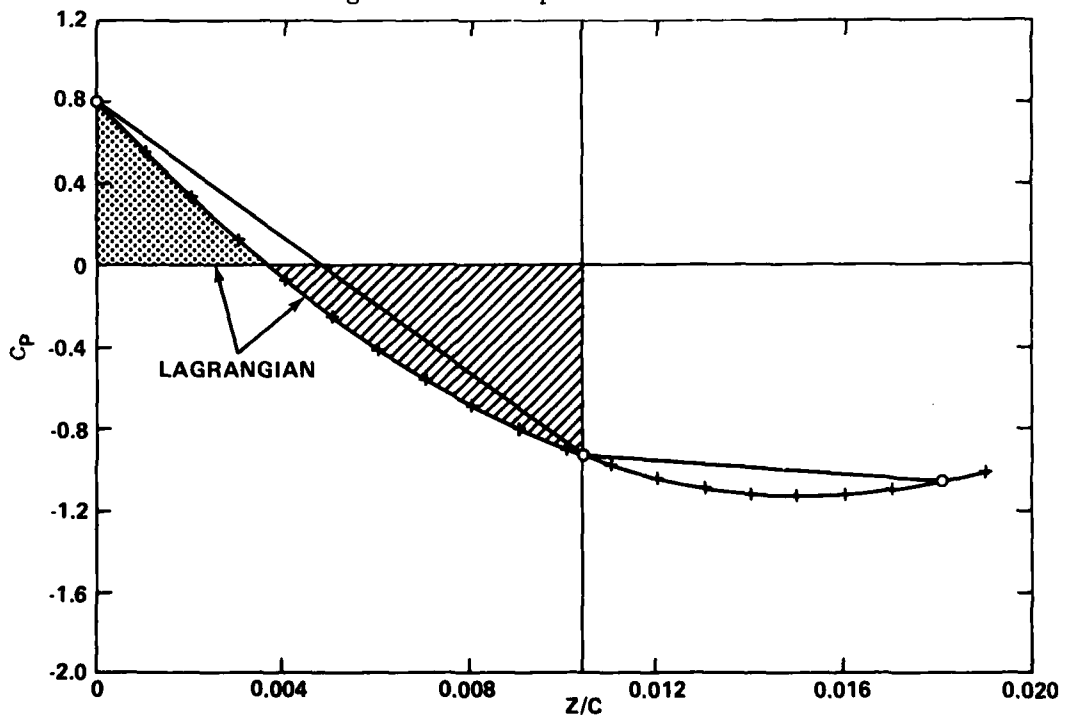


Figure 8b - Lagrangian Interpolations

Figure 8 - Integration of Pressure Drag

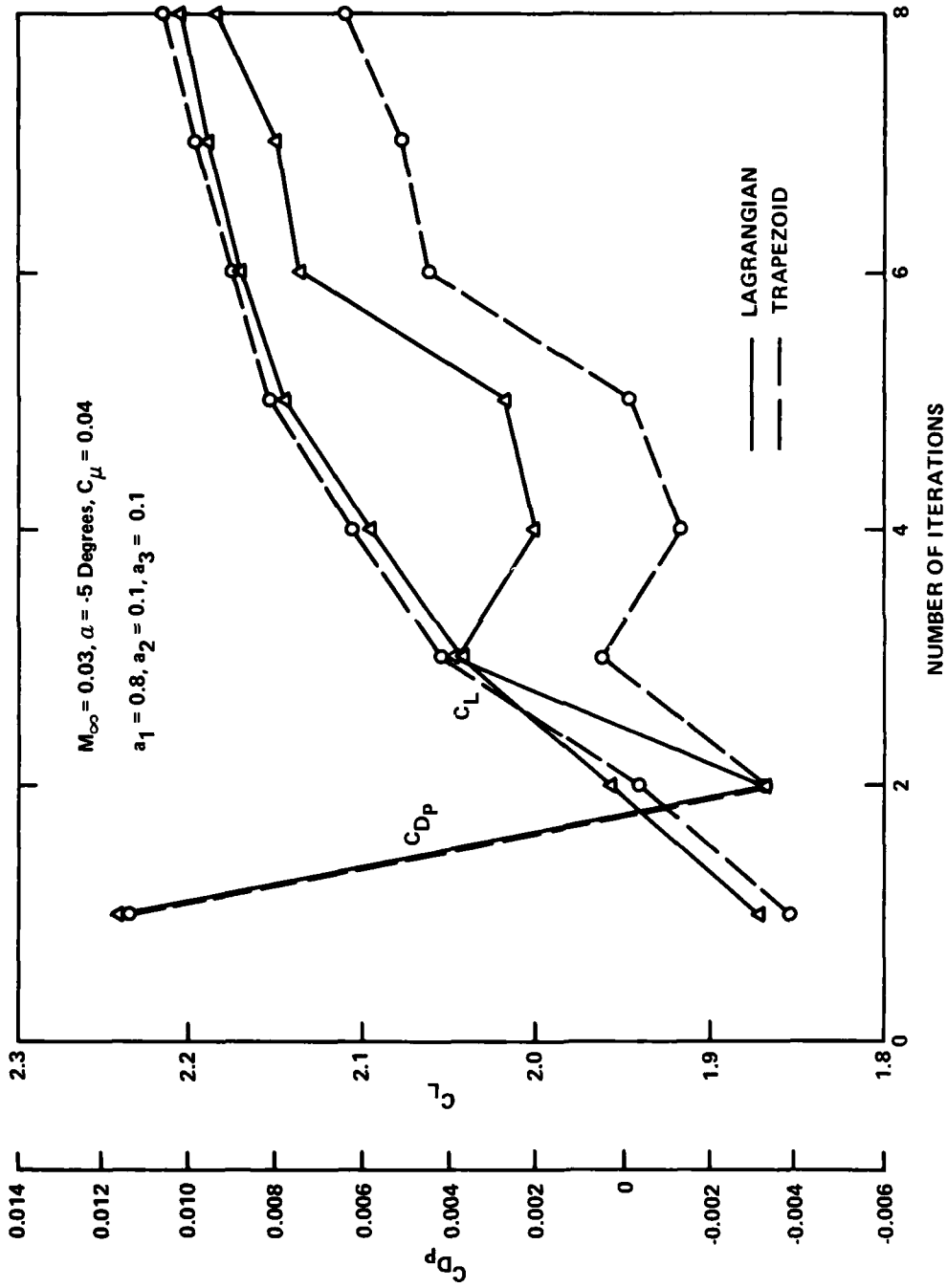


Figure 9 - Variation of Lift and Pressure Drag Coefficients During Iteration Process for Each Analysis

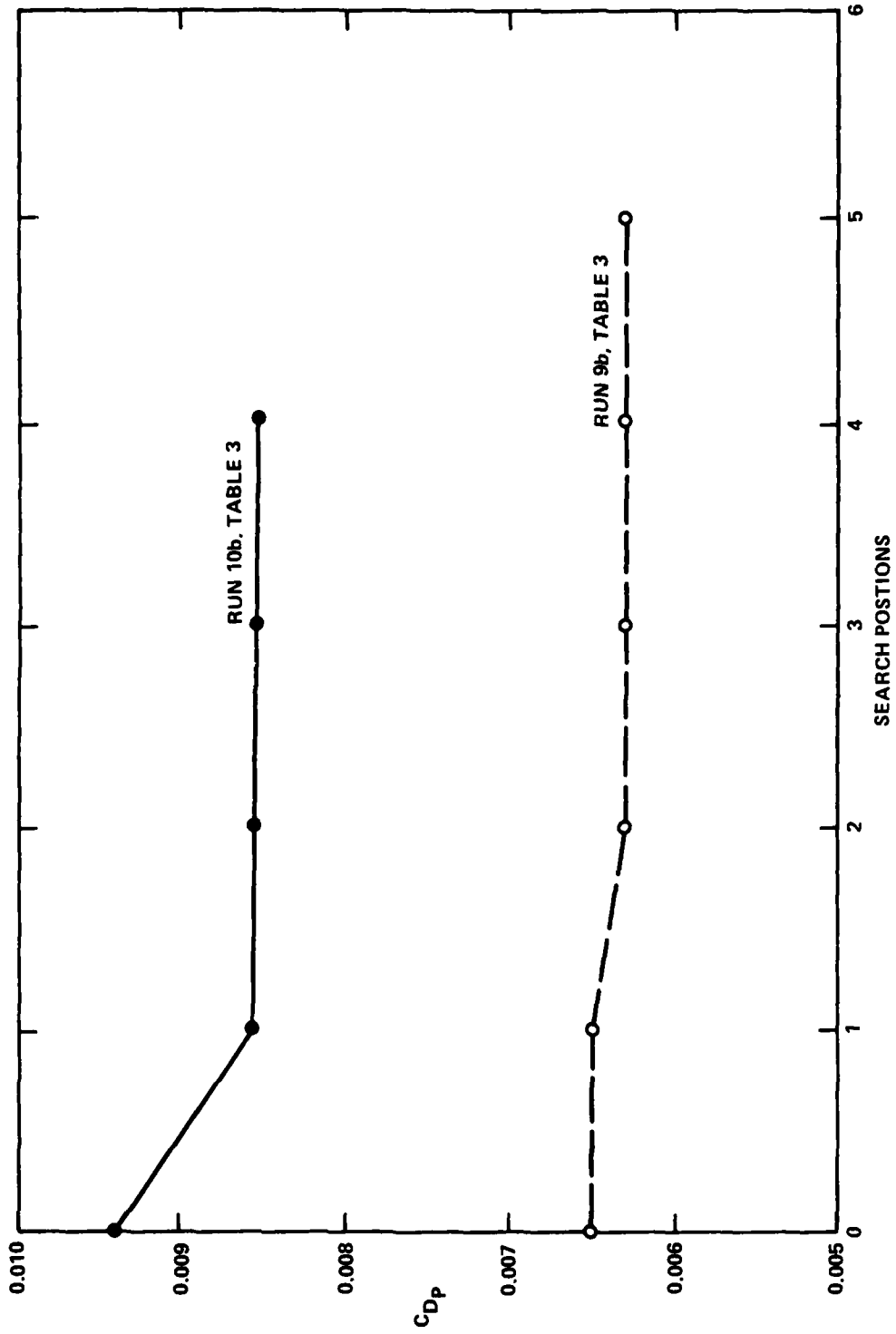


Figure 10 - Pressure Drag Coefficients During the Course of Optimization at $M_\infty = 0.3$, $C_\mu = 0.04$, and $\alpha = -5$ Degrees

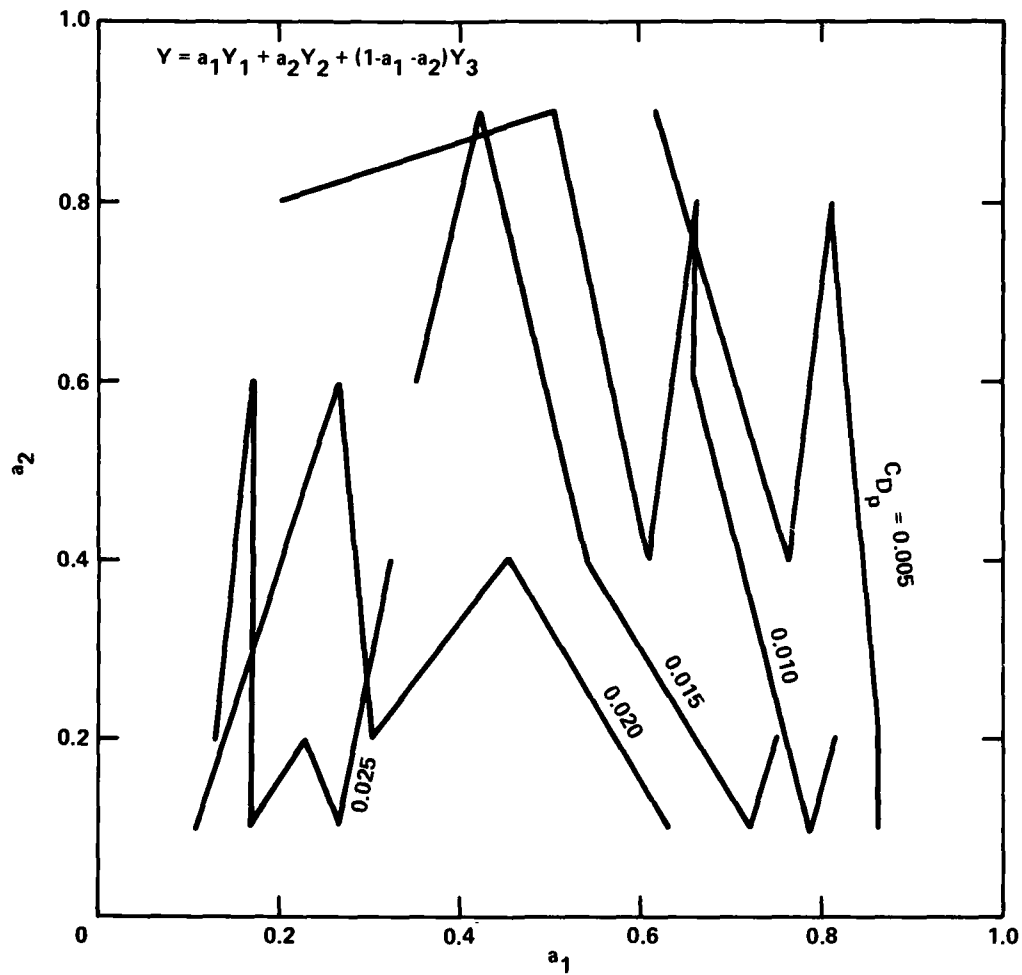


Figure 11 - Pressure Drag Coefficients in Two-Variable Space at $M_\infty = 0.3$, $C_\mu = 0.04$, and $\alpha = -5$ Degrees

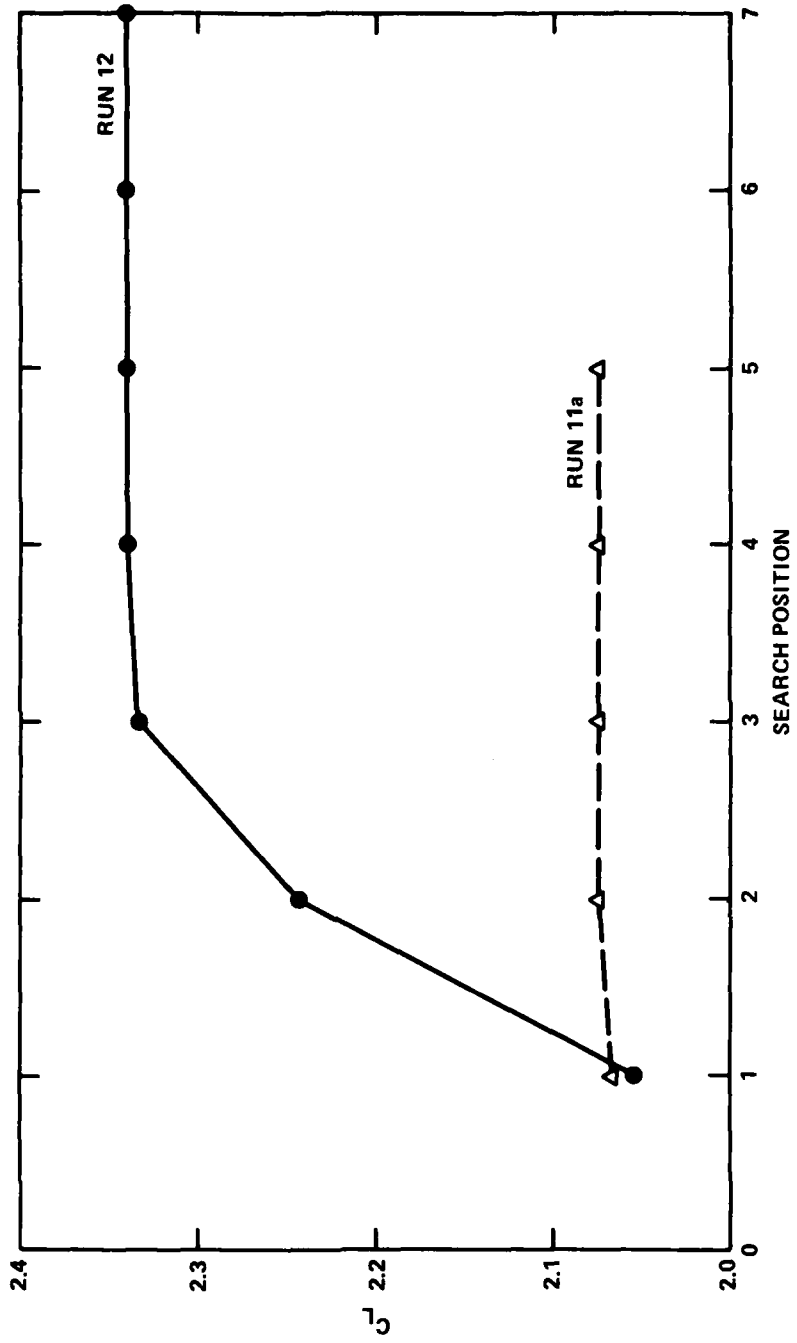


Figure 12 - Lift Coefficients During the Course of Optimization at $M_{\infty} = 0.3$,
 $C_{\mu} = 0.04$, and $\alpha = -5$ Degrees

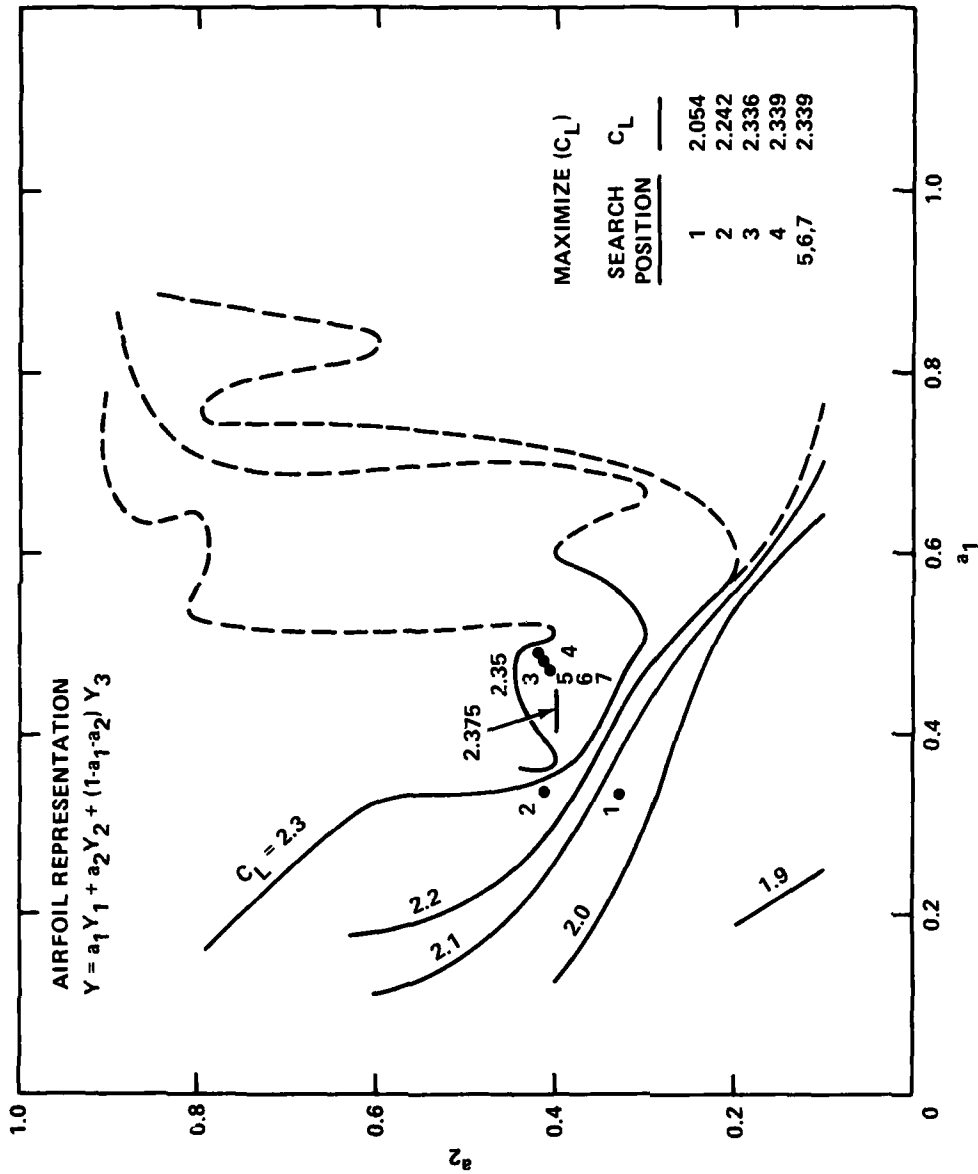


Figure 13 - Lift Coefficients in Two-Variable Space at $M_\infty = 0.3$, $C_\mu = 0.04$, and $\alpha = -5$ Degrees

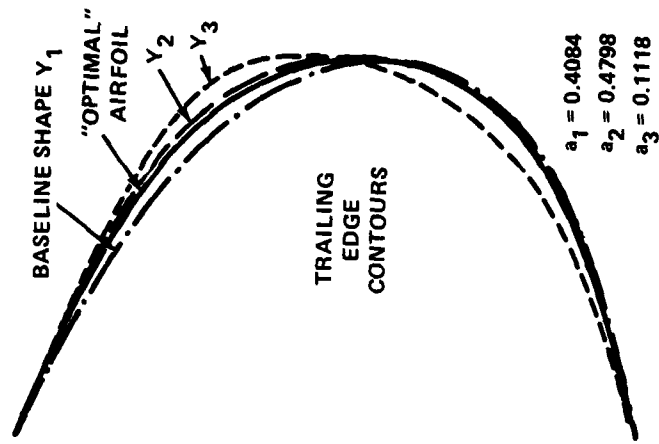


Figure 14 - "Optimal" Airfoil Shape Resulting from Maximizing C_L at $M_\infty = 0.3$, $C_\mu = 0.04$, and $\alpha = -5$ Degrees

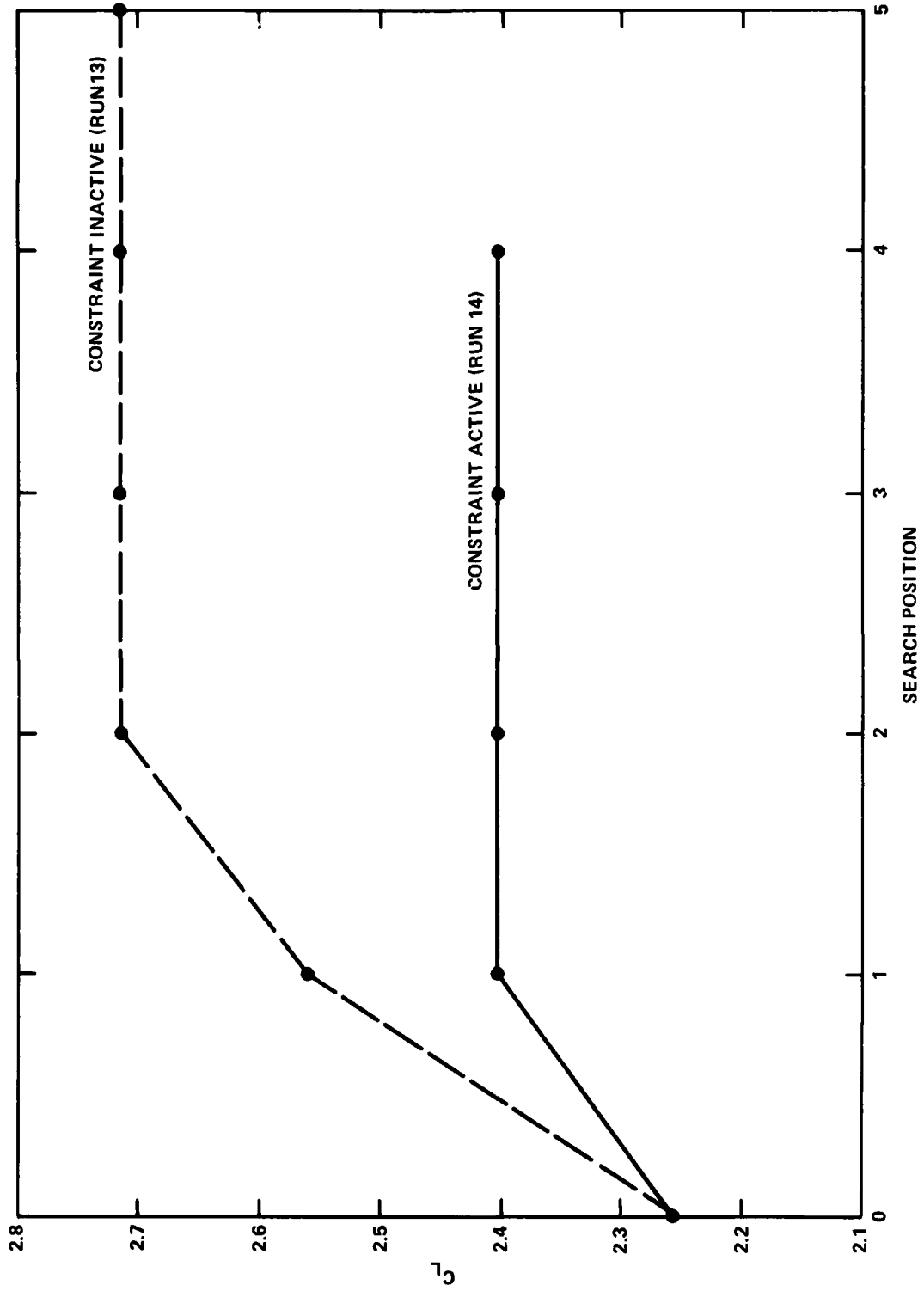


Figure 15 - Effect of Constraint in Optimization

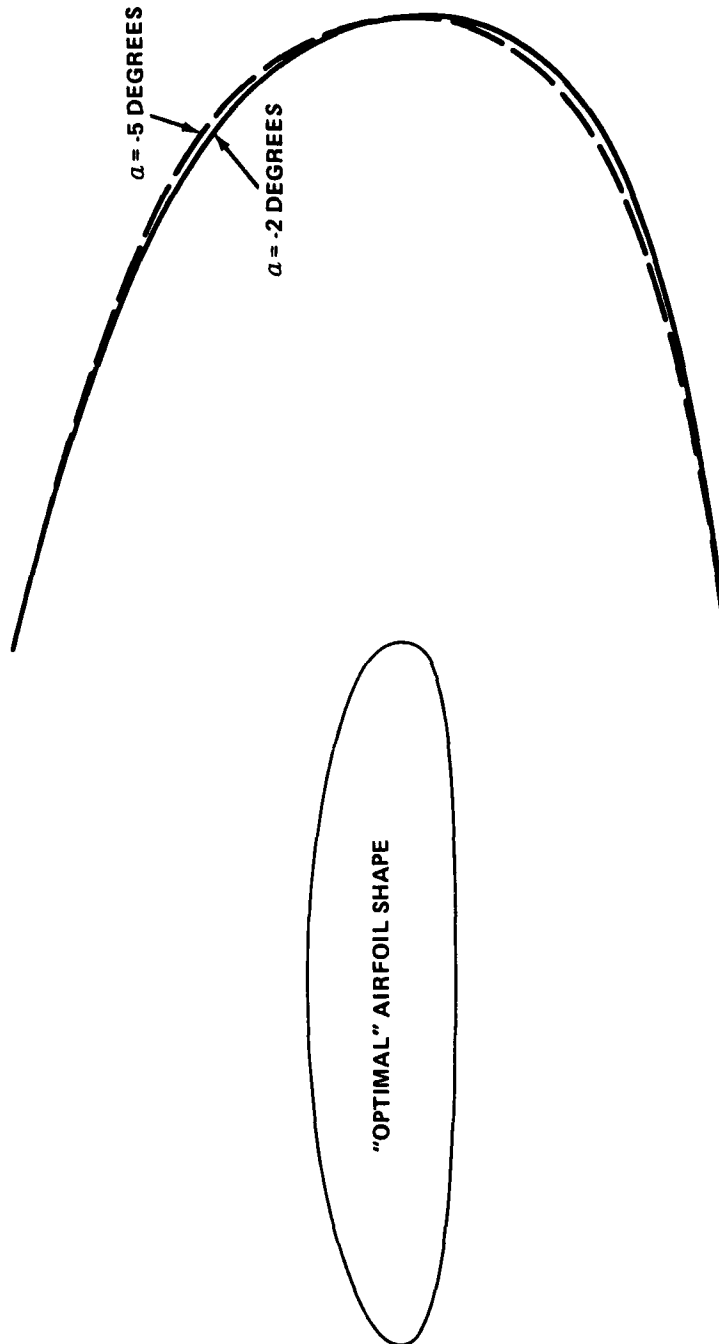


Figure 16 - "Optimal" Airfoil Shape Resulting from Maximizing C_L at $M_\infty = 0.3$,
 $C_\mu = 0.04$, and $\alpha = -2$ Degrees

TABLE 1 - LIFT AND DRAG COEFFICIENTS OF MODEL 103 CIRCULATION CONTROL AIRFOIL AT $M_\infty = 0.3$ AND $\alpha = -0.01$ DEGREE

Run	C_L	CIRCON Results				DTNSRDC Experiment (7 ft x 10 ft Transonic Wind Tunnel)		
		C_L	C_{D_p}	C_{D_f}	C_D	C_L	C_{D_p}	C_D
212	0.0073	0.6842	0.0048	0.0047	0.0022	0.4980	0.0084	0.0117
213	0.0105	0.8641	0.0079	0.0048	0.0021	0.7008	0.0148	0.0208
214	0.0111	0.8835	0.0115	0.0047	0.0051	0.7542	0.0181	0.0211
215	0.0160	1.1695	0.0067	0.0043	-0.0050	1.0932	0.0556	0.0236
216	0.0220	2.1620	0.0227	0.0044	0.0050	1.3634	0.1112	0.0413
217	0.0384	3.1714	0.0698	0.0043	0.0357	1.9203	0.1797	0.1106
218	0.0291	2.5010	0.0308	0.0046	0.0063	1.6575	0.1714	-

NOTES: 1. $(C_D)_{\text{Theory}} = C_{D_p} + C_{D_f} - C_L$

2. $(C_D)_{\text{Exp}}$ is obtained by integrating the wake rake survey, independent of surface pressure distribution.

3. C_L and C_{D_p} versus C_L are plotted in Figures 2 and 3.

TABLE 2 - COORDINATES OF BASELINE AIRFOILS

NUMBER OF AIRFOILS, NAFoil # 3
 NUMBER OF X-STATIONS, NXSTA # 30

X-LOCATIONS OF COORDINATES
 0.0000 .0050 .0200 .0400 .0700 .1000 .1500 .2000
 .2500 .3250 .4000 .5000 .5750 .6500 .7000 .7500
 .8000 .8500 .8750 .9000 .9250 .9500 .9600 .9700
 .9800 .9875 .9925 .9965 .9990 1.0000

BASIS VECTORS

VECTOR NUMBER 1
 BASIS AIRFOIL A

LOWER SURFACE COORDINATES
 .36085E-02 -.11485E-01 -.23991E-01 -.33318E-01 -.42415E-01 -.48795E-01 -.56277E-01 -.61410E-01
 -.65097E-01 -.68402E-01 -.70970E-01 -.72115E-01 -.71826E-01 -.70529E-01 -.69005E-01 -.66828E-01
 -.63803E-01 -.59615E-01 -.56927E-01 -.53708E-01 -.49534E-01 -.43420E-01 -.40048E-01 -.35872E-01
 -.30313E-01 -.24535E-01 -.19174E-01 -.12853E-01 -.60935E-02 .36000E-02

UPPER SURFACE COORDINATES
 .36085E-02 .17548E-01 .33288E-01 .46812E-01 .61805E-01 .73719E-01 .89564E-01 .10197E+00
 .11188E+00 .12288E+00 .12995E+00 .13389E+00 .13288E+00 .12846E+00 .12353E+00 .11687E+00
 .10828E+00 .97481E-01 .91070E-01 .83863E-01 .75162E-01 .63562E-01 .57696E-01 .50832E-01
 .42280E-01 .34066E-01 .26963E-01 .19180E-01 .11501E-01 .36000E-02

VECTOR NUMBER 2
 BASIS AIRFOIL B

LOWER SURFACE COORDINATES
 .36089E-02 -.11485E-01 -.23991E-01 -.33318E-01 -.42415E-01 -.48795E-01 -.56277E-01 -.61410E-01
 -.65097E-01 -.68402E-01 -.70970E-01 -.72115E-01 -.71826E-01 -.70529E-01 -.69005E-01 -.66828E-01
 -.63803E-01 -.59615E-01 -.56927E-01 -.54018E-01 -.49806E-01 -.43395E-01 -.39933E-01 -.35247E-01
 -.29085E-01 -.22475E-01 -.16590E-01 -.90999E-02 -.13898E-02 .89000E-02

UPPER SURFACE COORDINATES
 .36085E-02 .17548E-01 .33288E-01 .46812E-01 .61805E-01 .73719E-01 .89564E-01 .10197E+00
 .11188E+00 .12288E+00 .12995E+00 .13389E+00 .13288E+00 .12846E+00 .12353E+00 .11687E+00
 .10828E+00 .97481E-01 .91070E-01 .83863E-01 .75692E-01 .66235E-01 .61809E-01 .56373E-01
 .49356E-01 .42177E-01 .34969E-01 .27514E-01 .19944E-01 .89000E-02

VECTOR NUMBER 3
 BASIS AIRFOIL C

LOWER SURFACE COORDINATES
 .36085E-02 -.11485E-01 -.23991E-01 -.33318E-01 -.42415E-01 -.48795E-01 -.56277E-01 -.61410E-01
 -.65097E-01 -.68402E-01 -.70970E-01 -.72115E-01 -.71826E-01 -.70529E-01 -.69005E-01 -.66828E-01
 -.63803E-01 -.59615E-01 -.56927E-01 -.53747E-01 -.49401E-01 -.41828E-01 -.37491E-01 -.31649E-01
 -.23928E-01 -.16004E-01 -.83705E-02 -.10980E-03 .80892E-02 .19477E-01

UPPER SURFACE COORDINATES
 .36095E-02 .17548E-01 .33288E-01 .46812E-01 .61805E-01 .73719E-01 .89564E-01 .10197E+00
 .11188E+00 .12288E+00 .12995E+00 .13389E+00 .13288E+00 .12846E+00 .12353E+00 .11687E+00
 .10828E+00 .97481E-01 .91070E-01 .83863E-01 .75669E-01 .66082E-01 .61715E-01 .56952E-01

.51181E-01 .45743E-01 .40697E-01 .36647E-01 .27302E-01 .19477E-01

THIS PAGE IS BEST QUALITY PRACTICABLE
 FROM COPY FURNISHED TO DDC

TABLE 3 - RUN MATRIX FOR CIRCULATION CONTROL AIRFOIL OPTIMIZATION BASED ON BASELINE SHAPES Y_1 , Y_2 , AND Y_3

Run	Flow Conditions	Objective	Design Variables	Constraints	Results	Airfoil	Integration Scheme	Remarks
1	$M_\infty = 0.3$ $C_{\mu} = 0.04$ $\alpha = -5 \text{ deg}$	Sensitivity Study		-	Acceptable	Eq. (17)	Trapezoid	
2	$M_\infty = 0.3$ $C_{\mu} = 0.04$ $\alpha = -5 \text{ deg}$	Two-Variable Space		-	Acceptable	Eq. (17)	Trapezoid	
3	$M_\infty = 0.3$ $C_{\mu} = 0.04$ $\alpha = -5 \text{ deg}$	Two-Variable Space		-	Acceptable	Eq. (17)	Lagrangian	Figures 11 and 13
4	$M_\infty = 0.3$ $C_{\mu} = 0.04$ $\alpha = -2 \text{ deg}$	Two-Variable Space		-	Acceptable	Eq. (17)	Lagrangian	
5	$M_\infty = 0.135$ $C_{\mu} = 0.04$	Min (C_{Df})	α	$0.3 \leq C_L \leq 6.0$ $-10 \text{ deg} \leq \alpha \leq 0 \text{ deg}$ $a_1 = 0, a_2 = 1, a_3 = 0$	Slight change	Eq. (15)	Trapezoid	
6	$M_\infty = 0.135$ $C_{\mu} = 0.04$	Min (C_D)	α	$0.3 \leq C_L \leq 6.0$ $-10 \text{ deg} \leq \alpha \leq 0 \text{ deg}$ $a_1 = 0, a_2 = 1, a_3 = 0$	No change	Eq. (15)	Trapezoid	
7	$M_\infty = 0.3$ $C_{\mu} = 0.04$ $\alpha = -5 \text{ deg}$	Min (C_D)	a_1, a_2, a_3	$20 \leq C_L/C_{\mu} \leq 60$ $-0.2 \leq C_D/C_L \leq 0.7$ $0.2058 \leq t/c \leq 0.2062$ $-10 \text{ deg} \leq \alpha \leq 0 \text{ deg}$	No change	Eq. (15)	Trapezoid	
8	$M_\infty = 0.3$ $C_{\mu} = 0.04$ $\alpha = -5 \text{ deg}$	Min (C_{Dp})	a_1, a_2, a_3	$20 \leq C_L/C_{\mu} \leq 60$ $-0.2 \leq C_D/C_L \leq 0.7$ $0.2058 \leq t/c \leq 0.2062$ $-10 \text{ deg} \leq \alpha \leq 0 \text{ deg}$	No change	Eq. (15)	Trapezoid	
9a	$M_\infty = 0.3$ $C_{\mu} = 0.04$ $\alpha = -5 \text{ deg}$	Min (C_{Dp})	a_1, a_2	$50 \leq C_L/C_{\mu} \leq 60$ $-0.012 \leq C_D/C_L \leq -0.008$	No change	Eq. (17)	Trapezoid	$a_{10} = 0.3333$ $a_{20} = 0.3334$

TABLE 3 (Continued)

Run	Flow Conditions	Objective	Design Variables	Constraints	Results	Airfoil	Integration Scheme	Remarks
9b	$M_\infty = 0.3$ $C_\mu = 0.04$ $\alpha = -5 \text{ deg}$	Min (C_{Dp})	a_1, a_2	$50 \leq C_L/C_\mu \leq 60$ $-0.012 \leq C_D/C_L \leq -0.008$	Slight change	Eq. (12)	Trapezoid	$a_{10} = 0.8$ $a_{20} = 0.1$ Figure 9
10a	$M_\infty = 0.3$ $C_\mu = 0.04$ $\alpha = -5 \text{ deg}$	Min (C_{Dp})	a_1, a_2	$50 \leq C_L/C_\mu \leq 60$ $-0.014 \leq C_D/C_L \leq -0.008$	No change	Eq. (12)	Lagrangian	$a_{10} = 0.3333$ $a_{20} = 0.3334$
10b	$M_\infty = 0.3$ $C_\mu = 0.04$ $\alpha = -5 \text{ deg}$	Min (C_{Dp})	a_1, a_2	$50 \leq C_L/C_\mu \leq 60$ $-0.014 \leq C_D/C_L \leq -0.008$	Moderate change	Eq. (12)	Lagrangian	$a_{10} = 0.8$ $a_{20} = 0.1$ Figure 9
11a	$M_\infty = 0.03$ $C_\mu = 0.04$ $\alpha = -5 \text{ deg}$	Max (C_L)	a_1, a_2, a_3	$50 \leq C_L/C_\mu \leq 70$ $-0.2 \leq C_D/C_L \leq 0.7$ $0.2058 \leq t/c \leq 0.2062$	Slight change	Eq. (11)	Trapezoid	$a_{10} = 0.3333$ $a_{20} = 0.3334$ $a_{30} = 0.3333$ Figure 12
11b	$M_\infty = 0.03$ $C_\mu = 0.04$ $\alpha = -5 \text{ deg}$	Max (C_L)	a_1, a_2, a_3	$50 \leq C_L/C_\mu \leq 70$ $-0.2 \leq C_D/C_L \leq 0.7$ $0.2058 \leq t/c \leq 0.2062$	No change	Eq. (11)	Trapezoid	$a_{10} = 0.8$ $a_{20} = 0.1$ $a_{30} = 0.1$ Figures 12, 14
12	$M_\infty = 0.03$ $C_\mu = 0.04$ $\alpha = -5 \text{ deg}$	Max (C_L)	a_1, a_2	$50 \leq C_L/C_\mu \leq 60$ $-0.014 \leq C_D/C_L \leq -0.006$	Significant change	Eq. (12)	Lagrangian	$a_{10} = 0.3333$ $a_{20} = 0.3334$ $a_{30} = 0.3333$ Figure 15
13	$M_\infty = 0.3$ $C_\mu = 0.04$ $\alpha = -2 \text{ deg}$	Max (C_L)	a_1, a_2	$50 \leq C_L/C_\mu \leq 60$ $-0.014 \leq C_D/C_L \leq -0.006$	Significant change	Eq. (12)	Lagrangian	Figure 15
14	$M_\infty = 0.3$ $C_\mu = 0.04$ $\alpha = -2 \text{ deg}$	Max (C_L)	a_1, a_2	$50 \leq C_L/C_\mu \leq 70$ $-0.014 \leq C_D/C_L \leq -0.006$	Significant change	Eq. (12)	Lagrangian	Figures 15, 16

REFERENCES

1. Cheeseman, I.C., "The Application of Circulation Control by Blowing to Helicopter Rotors," The Aeronautical Journal, Vol. 71, No. 679 (Jul 1967).
2. Williams, R.M. and E.O. Rogers, "Design Considerations of Circulation Controlled Rotors," 28th Annual Forum of American Helicopter Society, AMC Paper 603, Washington, D.C. (May 1972).
3. Walters, R. et al., "Circulation Control by Steady and Pulsed Blowing for a Cambered Elliptical Airfoil," Aerospace Engineering Report TR-32, West Virginia University, Morgantown, W. Va. (Jul 1972).
4. Englar, R.J., "Two-Dimensional Transonic Wind Tunnel Tests of Three 15-Percent Thick Circulation Control Airfoils," NSRDC ASED Report 182 (Dec 1970).
5. Ambrosiani, J.P. and N. Ness, "Analysis of a Circulation Controlled Elliptical Airfoil," Aerospace Engineering Report TR-30, West Virginia University, Morgantown, W. Va. (Apr 1971).
6. Levinsky, E.S. and T.T. Yeh, "Analytical and Experimental Investigation of Circulation Control by Means of a Turbulent Coanda Jet," NASA CR-2114 (Sep 1972).
7. Dvorak, F.A. and R.J. Kind, "Analysis Method for Viscous Flow Over Circulation-Controlled Airfoils," Journal of Aircraft, Vol. 16, No. 1, pp. 23-28 (Jan 1979).
8. Wood, N.J., "The Aerodynamics of Circulation Controlled Aerofoils--A Progress Report," University of Bath, School of Engineering, England, Report 439 (Jan 1978).
9. Vanderplaats, G.N., "CONMIN--A FORTRAN Program for Constrained Function Minimization," NASA TM X-62282 (Aug 1973).
10. Dvorak, F.A. and F.A. Woodward, "A Viscous/Potential Flow Interaction Method for Multi-Element Infinite Swept Wings," NASA CR-2476 (Nov 1974).

11. Schlichting, H., "Boundary Layer Theory," 4th Edition, McGraw-Hill, New York (1960) pp. 147-151.

12. Curle, H., "A Two-Parameter Method for Calculating the Two-Dimensional Incompressible Laminar Boundary Layer," The Aeronautical Journal, Vol. 71 (Feb 1967).

13. Granville, P.S., "The Calculation of Viscous Drag of Bodies of Revolution," DTMB Report 849 (1953).

14. Nash, J.F. and J.G. Hicks, "An Integrated Method Including the Effect of Upstream History on the Turbulent Shear Stress," Proceedings of Computation of Turbulent Boundary Layer, AFOSR-IFP-Stanford Conference, Vol. 1 (1968).

15. Dvorak, F.A., "A Computer Program for the Viscous/Potential Flow Interaction Analysis of Circulation Controlled Airfoils," Analytical Methods Report 75-01, Bellevue, Washington (Apr 1975).

16. Fletcher, R. and C.M. Reeves, "Function Minimization by Conjugate Directions," British Computer Journal, Vol. 7, No. 2, pp. 149-154 (1964).

17. Zoutendijk, G.G., "Methods of Feasible Directions," Elsevier, Amsterdam (1960).

INITIAL DISTRIBUTION

Copies		Copies	
4	CNR	1	NAVSEASYSKOM
	1 211	1	NAVAIRPROPTTESTCEN
	1 430B	12	DTIC
	1 432		
	1 438		
4	ONR	1	AFOSR
	1 ONR Boston	1	USAFA
	1 ONR Chicago	1	AF INST TECH
	1 ONR London, England		
	1 ONR Pasadena	1	AFFDL
1	NRL	1	AEDC
1	USNA	9	NASA
6	USNPGSCOL	1	HQ, Washington, D.C.
	1 Lib	6	Ames Research Center/Lib
	5 Dr. G.N. Vanderplaats	1	Lib
		5	G.H. Kidwell
3	NADC	1	Langley Research Center
	1 AIR 07	1	Lewis Research Center
	1 AIR IV3, Dr. K.T. Yen		
	1 AIR 3015, C. Mazza	1	U of Akron/Lib
1	NWC/China Lake	1	Brown U/Div of Engr
1	NSWC/Dahlgren	2	Calif Inst of Tech
2	NSWC/White Oak	1	Grad Aero Labs
	1 Lib	1	Dr. T. Kubota
	1 Dr. T.F. Zien	2	Calif Inst of Tech/Jet
12	NAVAIRSYSKOM		Prop Lab
	1 AIR 03A	1	Lib
	1 AIR 03C	1	Dr. D.J. Collins
	1 AIR 03E	2	U of Calif/Berkeley
	1 AIR 03PA	1	Prof. M. Holt/Div Aero
	1 AIR 03PA3		Sciences
	1 AIR 310	1	Lib
	1 AIR 320D		
	1 AIR 5108	1	U of Calif/L.A.
	1 AIR 530B	1	U of Calif/LaJolla
	1 AIR 5301		
	1 AIR 954		
	1 PMA 269		

Copies

1 U of S. Calif/Lib
 1 Catholic U of America/Lib
 1 U of Cincinnati/
 Aerospace Engr
 2 Clemson U
 1 Dr. T. Yang/Mech Engr
 Dept
 1 Lib
 1 Cornell U/Lib
 1 Georgia Inst Tech/Lib
 1 Harvard U/Gordon McKay Lib
 1 Johns Hopkins U/Lib
 1 APL/Johns Hopkins U.
 1 U of Illinois/Lib
 2 U of Maryland
 1 Aerospace Engr
 1 Lib
 1 MIT/Lib
 2 U of Michigan
 1 Aerospace Engr
 1 Lib
 1 New York U/Courant Inst
 Math Sci
 1 U of N. Carolina/Lib
 2 N. Carolina State U/Raleigh
 1 Dr. F.R. DeJarnette/
 Mech & Aerospace Engr
 Dept
 1 Lib
 1 Pennsylvania State U/Lib
 1 Princeton U/Lib
 1 Purdue U/Lib

Copies

1 Stanford U/Lib
 2 U of Tennessee Space Inst
 1 Lib
 1 Dr. C.M. Wu
 1 U of Virginia/Alderman Lib
 2 Virginia Polytech Inst
 1 Carol M. Newman Lib
 1 Aero & Ocean Engr
 1 U of Washington/Lib
 1 W. Virginia U/Dept Aero Engr
 1 American Inst of Aeronautics
 & Astronautics
 1 Advanced Tech Ctr/C. Haight
 1 ARO Inc/Lib
 1 Bell Aerospace
 1 Boeing Company/Seattle
 1 Boeing Aerospace Co/Seattle
 1 Calspan Corp/Buffalo
 1 Douglas Aircraft Co/Lib
 1 Flow Research/Kent Washington
 1 General Dynamics/Convair
 1 General Dynamics/Fort Worth
 1 Grumman Aerospace Corp/Lib
 1 Hughes Aircraft Co/Lib
 1 Inst for Defense Analyses
 1 Lockheed-California/Lib
 1 Lockheed-Georgia Co/Lib
 1 Analytical Methods

Copies

1 Lockheed Missiles & Space Co/
Lib

1 LTV Aerospace Corp/Lib

1 McDonnell Douglas
St. Louis

1 Nielsen Engr & Res Inc

1 Northrop Aircraft

1 Rockwell International Corp/
Columbus, Ohio

1 TRW Systems Group/Lib

1 United Technology/
East Hartford, Conn.

CENTER DISTRIBUTION

Copies	Code	Name
5	012	
1	11	
1	15	
3	1603	
1	1660	
1	18	
1	27	
1	28	
10	5211.1	Reports Distribution
1	522.1	Lib (C)
1	522.2	Lib (A)
2	522.3	Aero Lib